9-1-1999

Measurement of residual stress in electrodeposited nickel films

Gary Richardson

Measurement of Residual Stress in Electrodeposited Nickel Films

By

Gary A. Richardson

A Thesis Submitted in Partial Fulfillment of the Requirements for the

Master of Science

In

Mechanical Engineering

Approved By:

_____Thesis Advisor
Dr. Surendra Gupta

_____
Dr. Robert Snyder

_____
Dr. Richard Budynas

_____Department Head
Dr. Satish Kandlikar

Department of Mechanical Engineering

College of Engineering

Rochester Institute of Technology

September 1999

Measurement of Residual Stress in Electrodeposited Nickel Films

I, Gary A. Richardson, hereby grant permission to the Wallace Library of the Rochester Institute of Technology to reproduce my thesis in whole or in part. Any reproduction will not be for commercial use or profit.

Date: 9/8/99 Signature of Author: _____

Acknowledgements

I would like to thank the following people who aided me throughout my research and in the preparation of this document:

Dr. Gupta for guidance and patience while serving as my advisor;

Dr. Budynas and Dr. Snyder for serving as thesis committee members;

Mike Gartley for assistance in the laboratory and with measurement techniques;

Berl Stein for ongoing advice and encouragement; and

All of my fellow co-workers at the Reflexite Precision Technology Center for continued support and assistance.

Table of Contents

List of Figures

List of Equations

Thesis Statement

For nearly as long as people have had the ability to create deposits by electrodeposition it has been known that the deposits are made in a state of internal stress. Throughout the past one hundred years several simple techniques used to measure these stresses have been developed. Unfortunately these methods have several shortcomings in both their formulation and interpretation, and seldom have the results from any of these tests been verified by another method. As electroplating becomes utilized to a greater extent in the high-tech applications of aerospace, optics, and electronics it is becoming ever more crucial to gain the ability to measure and understand the state of stress in a deposit. The intent of this research was to develop better means of modeling the deflection processes used in the simple testing techniques currently available and to verify the results of these measurements by x-ray diffraction, and these goals have been reasonably met. An improved numerical model of the deflection phenomenon associated with the change of length method was developed, and the results obtained by analyzing experimental data with this model were compared with calculations made by traditional models. In general, a strong correlation between the steady state stress values provided by each method was found to exist. Furthermore, when stress measurements obtained by the change of length method were compared to residual stress measurements made by x-ray diffraction of samples created under similar experimental conditions, a strong qualitative correlation between the two was found to exist.

Ch. 1 Introduction

1.1 Electroforming

Electroplating is a term that describes the electrochemical dissolution of a material from a source and its subsequent deposition onto a desired surface. A typical electroplating cell contains an anode, a cathode, and the electrolytic solution, which allows current to flow between the anode and cathode. The anode is composed of the sacrificial metal and is dissolved by the solution (usually a weak acid or an alkaline), placing ions of the anode material into the bath. As current flows through the cell, these ions migrate toward the cathode where they gain an electron and are added to the coating. The cathode is the surface on which the deposit is created, and it can be made of any conductive material that is not adversely affected by the solution in the cell.

Several terms commonly used to describe components or aspects of electroplating systems must be defined.

- Current Density: the amount of current flowing through one unit of surface area. Units are typically in Amperes per Square Decimeter or Amperes per Square Foot.
- Substrate: the cathode in the electrolytical cell, upon which material is deposited.
- Mandrel: the substrate in an electroforming process (see Figure 2), it constitutes the shape to be replicated.

The following table defines certain terms that pertain to the various stress measurement techniques that are relevant to this paper.

Figure 1: Electroforming Definitions

K:	Helix spring constant (N m/rad)
$\Delta\theta$:	Rotation of the helix due to deposit stress (rad)
p:	Helix pitch (m/rev)
t_s:	Substrate Thickness (m)
t_f:	Deposit ("film") Thickness (m)
E_s:	Substrate elastic modulus (Pa)
E_f:	Deposit elastic modulus (Pa)
ν_s:	Substrate Poisson's Ratio
ν_f:	Deposit Poisson's Ratio
l_s:	Substrate length (m)
Δ:	Change in substrate length due to deposit stress (m)
w:	Strip Width (m)
σ:	Average Deposit Stress (Pa)

In some cases, the process of electroplating may be used to create a separate, freestanding entity. This has become known as electroforming, and the ASTM Committee B8 has adopted the definition that "electroforming is the production or reproduction of articles by electrodeposition upon a mandrel or mold that is subsequently separated from the deposit" (ASTM Standard B374). Note that in this definition the separation of the electroform from the mandrel is emphasized, and therefore the electrodeposited metal must be sufficiently non-adherent to permit this separation. Additionally, there are inherent limitations to the geometry of the mandrel that is to be replicated, which are typically similar to those that occur in procedures such as injection molding. Figure 2 is an example of the use of electroforming to duplicate a structured surface (a Fresnel lens).

Figure 2: Electroforming Demonstration

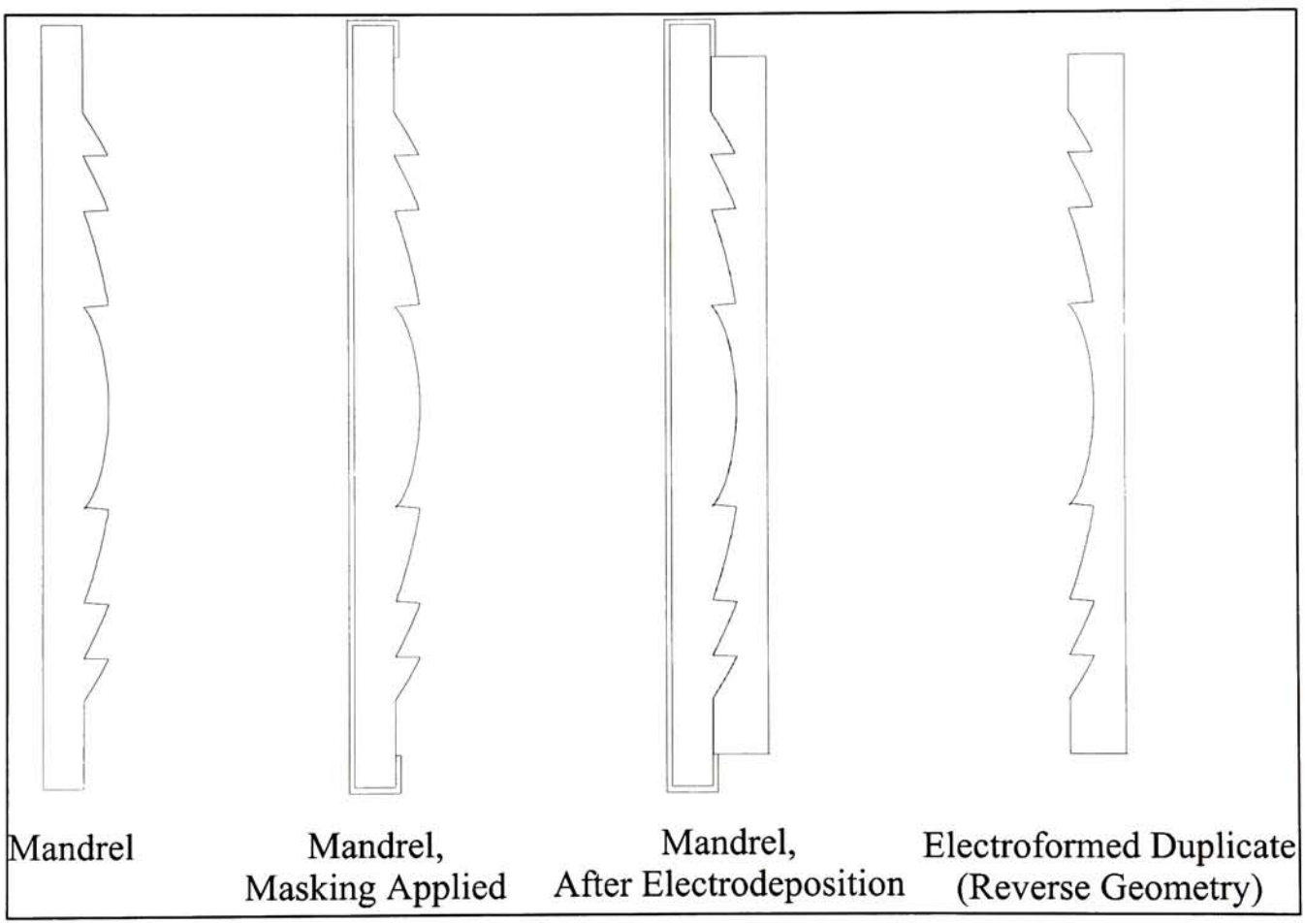

The process begins with a mandrel, which typically contains features that are to be duplicated. Here the front surface of the mandrel has been machined so that it has the pattern of a Fresnel lens on its face. Next, masking is applied to all surface area of the mandrel that will not be replicated. This will also allow for separation of the electroform when deposition is completed. At this point the mandrel is placed into the electroforming solution and contact is made to a DC power supply such that the positive lead is connected to the anode while the negative lead runs to the cathode, which in this case is the mandrel. When the power supply is turned on, current flows and the process of electrodeposition begins. At the point when a sufficiently thick deposit has been made, the mandrel is disconnected from the power supply and removed from the tank. It is then possible to separate the mandrel and the electroform, leaving a mirror-image replica of the original.

Alternatively, it is possible to electroform using a disposable mandrel. These are typically made of wax (covered with an electrically conductive coating) or aluminum (which can easily be dissolved with a caustic solution). In these situations the deposit material generally forms a shell around the outside of the mandrel, which is subsequently dissolved. This technique is often used in electroforming objects such as expansion bellows and wave guides.

The applications of electroforming are numerous and ever-increasing. Electroforming is well suited to creating parts with complicated surface features, parts that could not easily be mass-produced any other way. An ideal example of this

is the manufacture of wave-guides. Electroforming is also useful in replicating surfaces with minute mechanical features. This property is often utilized in the production of microstructured optical patterns such as those on Fresnel lenses and cube-corner retroreflectors. Finally, it is possible to produce very specific material properties through the process of electroplating. One can obtain electroforms with specific material properties such as hardness, ductility, elastic modulus, and magnetic character, which makes electroforming an ideal technique for use in the high-tech fields of aerospace and microelectronics.

1.2 *Stresses in Electroforming*

An inherent aspect of the electroforming process is that all electroplated materials are deposited in a state of internal stress. The origins of deposit stress are not well understood at the present time, in fact several plausible theories relating to this matter have been presented. It has been suggested that internal stress may be due to a crystal lattice mismatch between the substrate and deposit, as the deposited atoms will try to mimic the structure of the surface onto which they fall [1]. Stresses may also arise because of the effect that impurities in the deposit material have on its crystal structure. These topics will not be further discussed here as this work pertains to a better means of measuring these stresses, rather than understanding their nature.

Internal stress represents an important factor in practical electroforming. In cases where miniature surface features are to be replicated, deposit stress affects the dimensional stability of the electroform upon separation from the mandrel. Deposit stress can also cause some types of surface geometry to effectively "lock" the electroform onto the mandrel, which often results in the loss of both. Finally, in extreme cases, high internal stresses can result in cracking or premature separation of the electroform while plating is still occurring.

Almost any attribute of the solution in an electroplating bath will have an effect on the stress level of the deposit. Some of the most critical factors are temperature, current density, deposit thickness, pH, and the concentration of many

different additives common to electroforming baths.

1.3 Traditional Measurement Techniques

The most common means of measuring deposit stress in an electroforming solution are based upon the same principle: a thin substrate is plated and the resulting changes in the size or shape of the substrate are monitored. In some cases (the "Bent Strip" method and the Spiral Contractometer), a deposit is made onto one side of a thin strip of metal while the other side is masked with an insulating layer. Any stress in the deposit will result in a change in curvature of the strip. Similarly, if both sides of the same strip were plated any deposit stress would result in a net change in the length of the strip (the I.S. Meter is based upon this principle).

The Spiral Contractometer

Theory

Since its development in 1949 by Brenner and Senderoff [2], the Spiral Contractometer has become the preferred instrument used to measure stresses in electrodeposits in an industrial setting. The primary component of the device is a strip of stainless steel formed to the shape of a helix. The internal side of the helix is coated with a lacquer or a layer of *Teflon* while the external side remains bare, allowing it to be plated. During the plating cycle, stresses in the electrodeposit will cause the helix, one end of which being fixed, to deform. Compressive stresses

will result in a tightening of the helix while tensile stresses will cause it to unwrap. The angular deflection of the free end of the coil is transferred to a pointer by a set of gears and can be monitored throughout the testing process on a dial mounted atop the coil. This information may be converted to a sort of 'average' stress in the following manner.

Equation 1: Spiral Contractometer Average Stress Calculation

$$\sigma = \frac{2 \cdot k \cdot \Delta\theta}{p \cdot t_s \cdot t_f}$$

K:	Helix spring constant
$\Delta\theta$:	Rotation of the helix due to deposit stress
p:	Helix pitch
t_s:	Substrate Thickness
t_f:	Deposit ("film") Thickness
σ:	Average Deposit Stress

Operation

Figure 3: The Spiral Contractometer

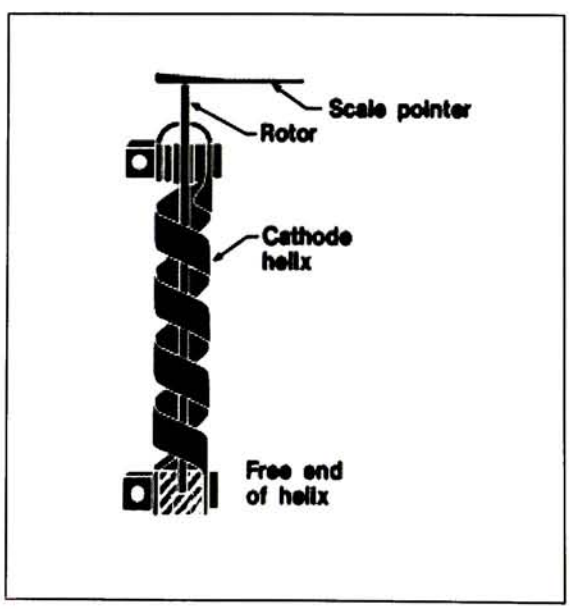

The spiral contractometer is a rather difficult and time-consuming instrument to operate. The setup includes determining the spring constant of the helix, fastening the helix to the instrument, masking the top and bottom regions of the helix to prevent plating and centering the pointing device on the scale. If the manufacturer's instructions are to be followed, it is necessary to utilize a beaker and a hot plate in order to operate the test externally to the plating tank.

The Bent Strip

Figure 4: The Bent Strip Test

Theory

Developed by G. G. Stoney in 1909 [3], the bent strip technique is probably the most straightforward and simple means of measuring stresses in electrodeposits.

It works in the following manner: a thin strip of metal is plated on one side while a protective lacquer coats the other. Any stresses in the deposit will cause a net curvature to be induced upon the strip, and this curvature can be converted to an equivalent average stress level with the following equation:

Equation 2: Bent Strip Stress Calculation

$$\sigma = \frac{E_s}{6 \cdot (1-\upsilon)} \frac{t_s^{\,2}}{t_f} \frac{\Delta\theta}{l_s}$$

t_s:	Substrate Thickness
E_s:	Substrate elastic modulus
ν:	Substrate Poisson's Ration
l_s:	Substrate length
$\Delta\theta$:	Angular Deflection of Substrate due to deposit stress
w:	Strip Width
σ:	Deposit Stress
t_f:	Deposit Thickness

Operation

The Bent Strip test is extremely simple and easy to carry out. One of its most attractive features is the fact that the test can be performed directly in a plating tank [4]. The measurement is generally performed with a 0.002" beryllium copper strip which has two legs, each with one side coated to prevent plating. The strip is placed into a specially designed tubular test cell that is fastened to the edge of the plating tank. The cell's functions are to prevent the strip from solution flow disturbances, to create an electric field conducive to uniform deposit thickness distribution across the

strip and to constrain the ends of the strip during testing. After being affixed to the test cell, the strip is plated for a given amount of time. Since the bare sides of the strip legs face opposite directions, a stressed deposit will result in a net spread with each of the legs bending either toward (compressive deposit) or away (tensile) from its exposed surface. After plating is completed, one simply measures the resulting spread and determines the deposit stress by the Equation 2.

Change of Length Method

Figure 5: The I.S. Meter

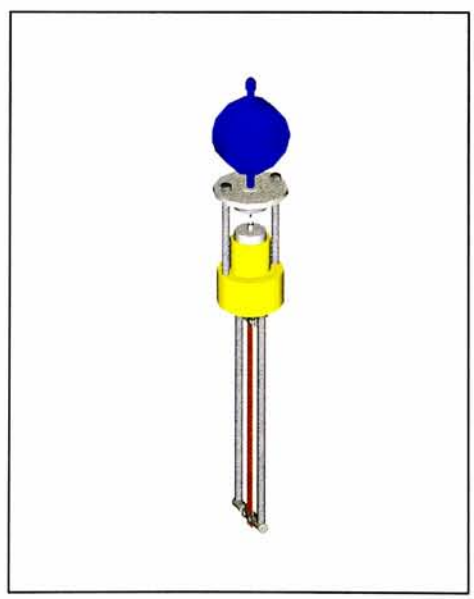

Theory

The concept behind this method, first proposed by M. Ya Popereka in 1958 [5], is fairly straightforward: a thin strip of metal is kept in tension by a given

preload while being plated on both sides. Any inherent stress in the deposit will cause a change in the length of the strip. This change is measured by keeping one end fixed and allowing the free end to move and affect a gauge attached to it. There does exist some disagreement about the mathematical model that should be utilized to determine stress from this length change.

Each of the traditional models shares the assumption that the deposit contracts or expands as if affected by a constant stress acting along its axis. This stress is equivalent to a force distributed equally over the cross-section of the deposit. In a real sense, such a distributed force does not exist. The closest correlation to this 'stress' would be the hydrostatic pressure acting in the deposit, namely the average of the principal stresses. For the purpose of comparing readings taken by the I.S. Meter to those obtained by X-ray diffraction the comparison will be made with the average of the principal stresses acting in the plane parallel to the sample surface, as the stress perpendicular to the sample surface is assumed to be zero.

The following is the most basic derivation of a formula used to calculate the average stress in a deposit for the change of length method, which was first presented by Dvorak and Vrobel [6].

Figure 6: Derivation for the Change of Length Method

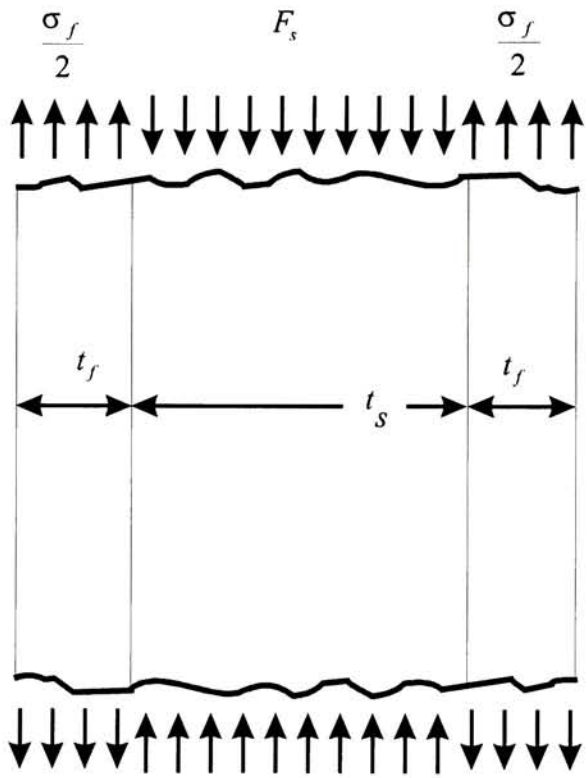

In this model, the instantaneous stress level of the deposit is assumed to be constant throughout the plating process. Here the assumption of a state of plane strain is not made, and the effects of lateral contraction are ignored.

By summing forces in the vertical direction, it is possible to calculate the equivalent force exerted by the film stress acting through the deposit thickness on the substrate (assuming that the deposit thickness is much smaller than the strip

thickness).

$$F_s = 2\sigma \cdot w \cdot t_f$$

It is then possible to express the net deflection in terms of the equivalent force F_s using basic mechanics of materials techniques. This expression is of the form:

$$\Delta = \frac{F_s l_s}{t_s w E_s}$$

Substituting for the equivalent force F_s and solving for σ yields:

Equation 3: Dvorak and Vrobel's Formula for Average Stress

$$\sigma_f = \frac{\Delta E_s t_s}{2 \cdot l_s t_f}$$

t_s:	Substrate Thickness
t_f:	Deposit ("film") Thickness
E_s:	Substrate elastic modulus
l_s:	Substrate length
Δ:	Change in substrate length due to deposit stress
σ_f:	Average Deposit Stress

This is an expression for the average stress in the deposit given the previously stated assumptions.

It is also possible to develop a formula that takes into account the stiffening of the substrate that occurs during plating, and this was first accomplished by M. Ya. Popereka [5]:

Popereka assumes that a state of plane strain exists in this process, and for this reason the elastic modulii are corrected accordingly.

$$\tilde{E}_s = \frac{E_s}{(1-\upsilon_s)} \qquad \tilde{E}_f = \frac{E_f}{(1-\upsilon_f)}$$

For the sake of simplicity it is assumed that Poisson's ratio for both the substrate and deposit are equal, or:

$$\upsilon_f = \upsilon_s$$

Therefore:

$$\tilde{E}_s = \frac{E_s}{(1-\upsilon_f)}$$

Additionally, the following substitution is made to simplify the derivation:

$$D = w\left(E_s t_s + 2E_f t_f\right)$$

The following figure demonstrates the model used in this derivation:

Figure 7: Derivation of Popereka's Equation

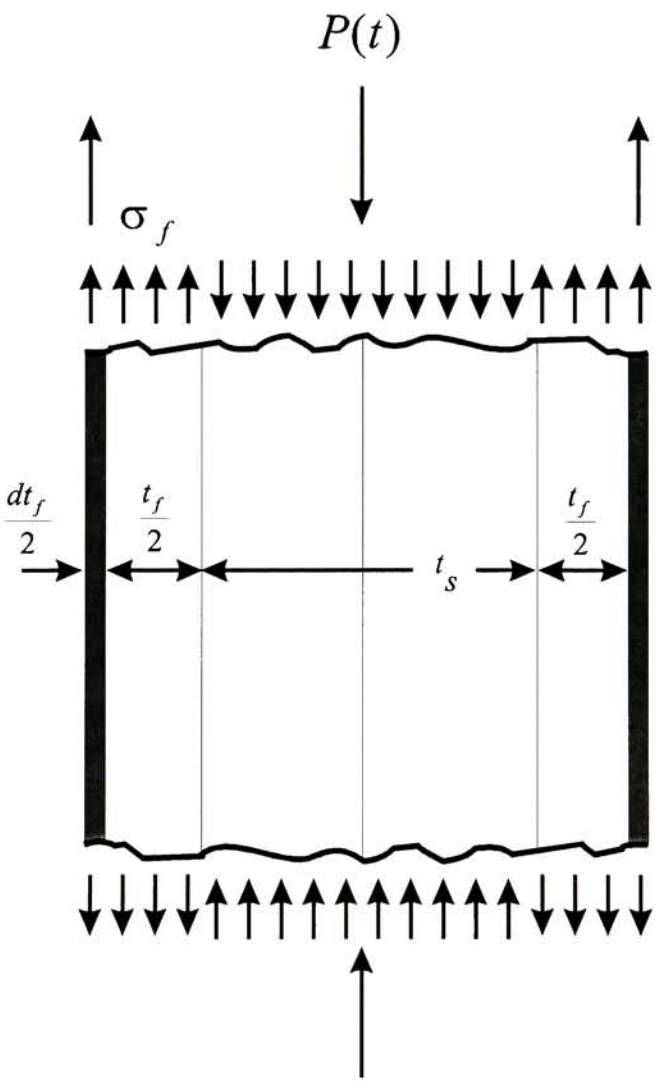

By summing forces in the vertical direction for a differential layer of the deposit, the force exerted by stress in the layer can be expressed in terms of the stress in the layer:

$$dP = \sigma \cdot w \cdot dt_f$$

It is then possible to express the net deflection in terms of the equivalent force P using basic mechanics of materials techniques. This expression is of the form:

$$\Delta = \frac{Pl_s}{D}$$

Differentiating this equation yields:

$$d\Delta = l_s\left(\frac{dP}{D} - \frac{PdD}{D^2}\right)$$

Eliminating the inverse square term as it is much smaller than the first term gives:

$$d\Delta = l_s\left(\frac{dP}{D}\right)$$

The original equation for dP can now be substitute, and solving for the average stress σ yields:

$$\sigma = \frac{D}{wl_s} \cdot \frac{d\Delta}{dt_f}$$

Substituting for D and simplifying results in the following:

$$\sigma = \frac{\tilde{E}_s t_s + 2\tilde{E}_f t_f}{l_s} \cdot \frac{d\Delta}{dt_f}$$

Finally, the assumption that a linear relationship between Δ and t is made ($d\Delta/dt_f=\Delta/t_f$), and remembering that the total deposit is twice the amount deposited on each side ($2t_f$), we get the final version of Popereka's equation.

Equation 4: Popereka's Formula for Average Stress

$$\sigma = \frac{\Delta\left(\tilde{E}_s t_s + 2\tilde{E}_f t_f\right)}{2l_s t_f}$$

t_s:	Substrate Thickness
t_f:	Deposit ("film") Thickness
E_s:	Substrate elastic modulus
E_f:	Deposit elastic modulus
l_s:	Substrate length
Δ:	Change in substrate length due to deposit stress
σ_f:	Average Deposit Stress

In order to obtain this closed-form equation it was assumed that PdD/D^2 was very near zero. This would require that Δ/ℓ is on the order of magnitude of 10^{-10}. In the practical application of this model to a real-world stress measuring device this criterion is generally not met because in order to obtain a significant deflection electrodeposition must be allowed to occur until the deposit thickness is no longer negligible when compared to the substrate thickness. Since the error in measurements associated with these devices is generally quite large when compared to the discrepancy caused by the eliminated term, it does not constitute a significant problem.

Although not entirely sound in the purest of mathematical terms [7], this formula provides a very useful correction. As deposit thickness increases, less deflection occurs with the same amount of deposit stress; therefore using the first formula will result in calculated stress values that will asymptotically approach zero. Also note that Popereka's formula assumes a state of plane stress which requires that the elastic modulii be corrected by the factor $1/(1-\nu)$, where ν is Poisson's ratio. For nickel-on-copper deposition, this serves to increase the calculated stress value by approximately 40%.

The difference in calculations between these two models is displayed in Figure 8. This chart contains data taken from an I.S. Meter test and analyzed with Dvorak and Vrobel's formula as well as Popereka's formula. Calculated stress values are plotted against the 'sandwich' thickness of the substrate/deposit conglomerate,

which consists of the substrate and the electrodeposited material on either side of it. This practice will be maintained throughout the work.

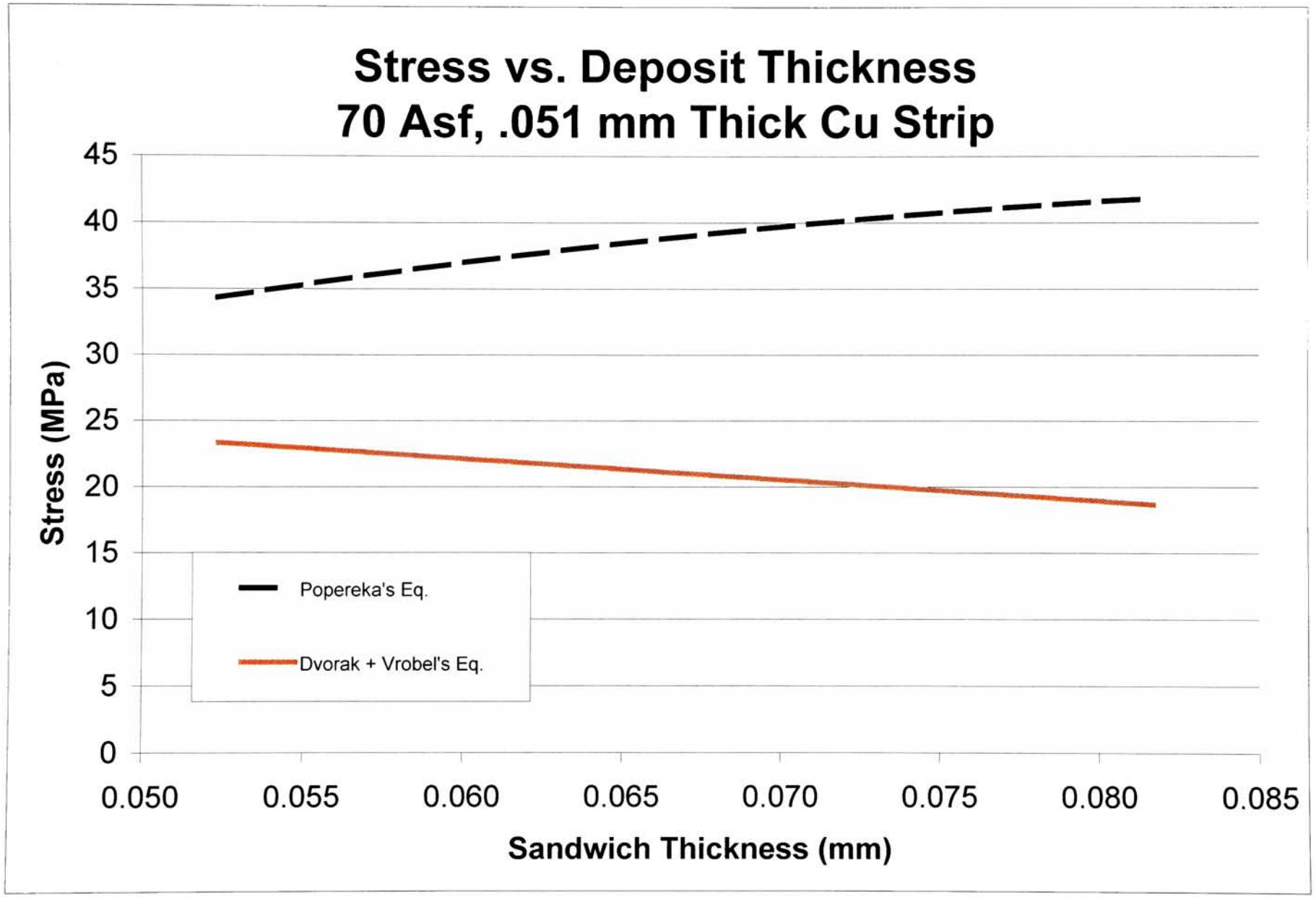

Figure 8: Stress vs. Thickness, Traditional Analysis

Initially, the average stress values calculated by both formulas differ by a constant scaling factor. This is due to the fact that early on, the deposit thickness is rather negligible, and therefore the only significant difference between the two formulae is the factor of $1/(1-\nu)$ applied to Equation 4. The numerical significance is that the initial average stress calculated by Popereka's formula is approximately 140% of the average stress as calculated by Dvorak and Vrobel's equation.

As the deposition process continues the effects of the second term in Popereka's formula, which takes into account the stiffening of the substrate by the deposit material, becomes increasingly significant. Because Dvorak and Vrobel's equation ignores this term, the corresponding stress values gradually decrease throughout the testing process. As the 'sandwich' thickness increases in time, the calculated stress values will asymptotically approach zero. Alternatively, stress values calculated by Popereka's formula exhibit an altogether different behavior. Instead of falling off in time, they gradually increase. This phenomenon is typical of data processed in this manner, and a few observations are readily made. Most notable is the fact that if deposit stress does become constant with increased thickness (as is most likely the case in reality) then neither of these models accurately portrays the process. Clearly this simplified approach in modeling is not adequately representative of the behavior of the deposition process.

Ch. 2 Stress Analysis with the I.S. Meter

2.1 Basic Design and Operation

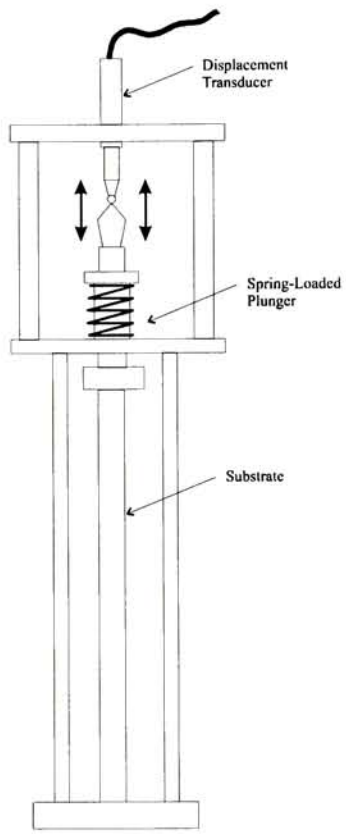

Figure 9: Schematic of the I.S. Meter

As previously stated, the I.S. Meter is based upon the change of length method. A thin strip of metal is clamped into the instrument, one side is held rigidly while the other is attached to a spring-loaded floating piston. The piston is used to hold the strip in a state of tension throughout the testing process, and since the spring constant is very small when compared to the stiffness of the strip the preload force

may be considered constant and therefore ignored.

During the plating cycle, any stress occurring in the deposit will cause a change in the length of the test strip. A displacement transducer is kept in contact with the top of the piston, which allows measurements of the length change to be taken throughout the plating process. Commonly used instruments in such situations, displacement transducers provide an output voltage proportional to the axial location of a spring-loaded pointer. The I.S. Meter, as used for this research, is detailed in Figure 9.

For this research, gage blocks were used to calibrate the transducer to an accuracy of +/- .00001 in. The performance of the transducer was then verified using a milling machine with a digital readout having an accuracy of +/- .0001 in. The output of the transducer agreed with the readout to the expected four decimal places. Furthermore, the output was almost linear over the short ranges used for measurements taken in this research. Readings were taken every five seconds during testing by an automated computer control program using an analog input board to measure the voltage output of the transducer.

2.2 *Specifics of Testing*

As current density has a direct impact on deposit stress level, variation in this parameter was used to achieve the range of stress values studied in this investigation. The following figure demonstrates the relationship between stress and current density for a typical electroforming solution.

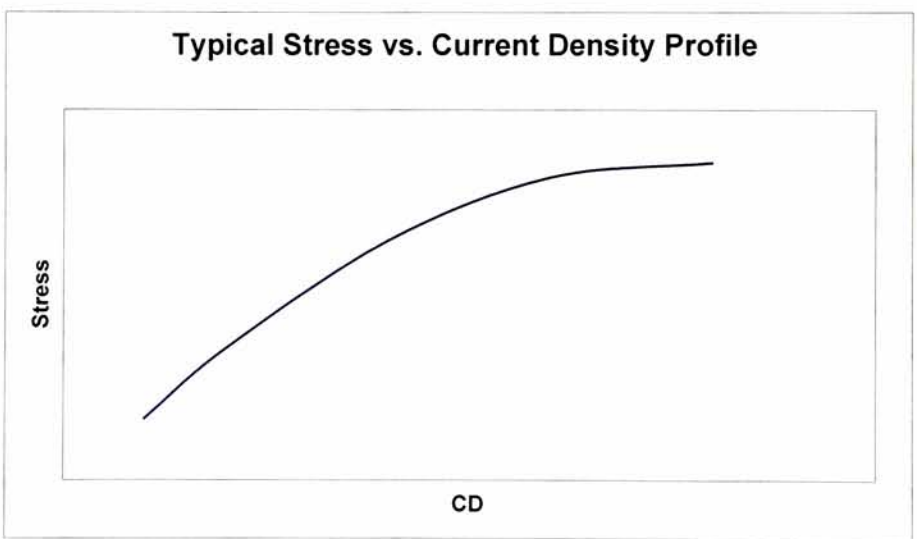

Figure 10: Stress vs. Current Density Profile

Typical current densities used ranged from 15 to 45 Amps per square foot, and plating time was set accordingly to achieve a constant deposit thickness for all specimens.

In performing the tests with the I.S. Meter, care had to be taken not to allow stress in the test strip to exceed its yield stress. Since deposit stress was typically in the range of +/-35 MPa, plating thicknesses had to be chosen so as to insure that stress in the test strip remained less than about half the yield stress of the strip. Another factor that becomes relevant is the thickness of the strip used in the instrument. Here there is a tradeoff between resolution and test duration, since a thinner strip will yield greater deflections than a thick strip will. For this research, a strip of 0.05-mm thickness was chosen. This provided a reasonable resolution while still allowing tests to be made to the deposit thicknesses required. The other dimensions of the strip were dictated by the design of the I.S. Meter: they are approximately 10 mm wide by 200 mm long.

As a general rule in electroplating, abrupt changes in the surface geometry of a substrate cause uneven thickness distribution. Obviously, if the thickness of plated material is not constant across the substrate profile, it follows that current density varied as well. Since current density has such a pronounced impact on deposit stress, coating thickness must be made as uniform as possible in order to attain an accurate measurement of stress at a given current density.

Looking at a two-dimensional cross-section view of a substrate, it is possible to predict the approximate shape a deposit will take. Sharp angular discontinuities cause the most drastic variations in deposit thickness: small included angles generally cause a deposit to be very thin in the "valley" and thicker on the top edges

while deposits build up dramatically around larger angles (see Figure 11 A and B).

Figure 11: Plating Distribution

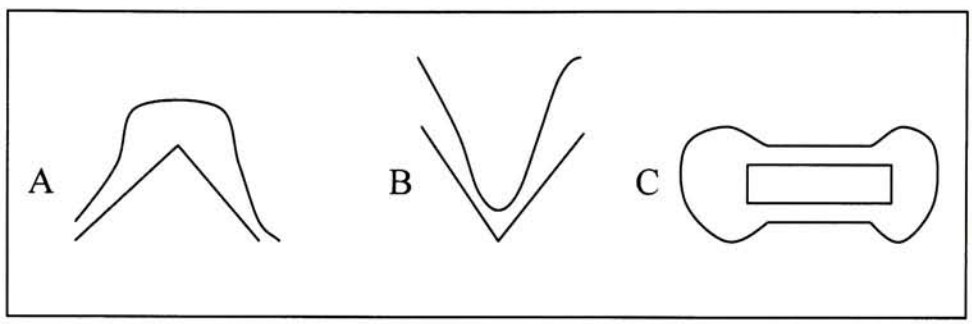

In the case of the I.S. Meter, the substrate has a rectangular cross-section. Electroplating on such a substrate results in a cross-sectional shape resembling a "dogbone" (see Figure 11C). Furthermore, as the deposit becomes thicker this effect becomes more and more pronounced, which again means increased variation in current density across the surface. Since the modeling used to calculate stress in this deposit assumes plating occurs only on the front and back of the strip, any plating on its edges contributes to an error in measurement.

Fortunately, it was possible to minimize this effect. The design of the I.S. Meter itself helps to give a more even thickness distribution, as the support rods on each side of the strip serve to shield the high current density regions on the edges. This affects the electromagnetic field characteristics and inhibits ion flow to the sides

of the strip while not affecting the plating that occurs on its front and back. Secondly, by using a more accurate means of measuring the change in strip length through the plating process it was possible to reduce the length of plating time for each test with the instrument. Furthermore, it can be assumed that minor variations in deposit thickness are "averaged out" in the situation that results. Since the relationship between stress and current density is approximately linear in most cases, the thicker regions at the edges will have been deposited in a state of high internal stress relative to less thick regions on the front and back of the strip. It can be assumed that these effectively cancel one another out, so long as the deposit is kept relatively thin.

An attempt was made to prepare all specimens in the same manner with regards to location and orientation. The I.S. Meter was positioned so that the short axis of the strip was parallel to the anode surface. The reasoning was that each side of the strip should be plated under identical conditions, and if one side faced the anode while the other faced the back of the plating tank this would not be possible. Finally, the I.S. Meter was placed approximately 10" from the anode basket, and this distance was maintained throughout the research.

The substrate for testing both in the I.S. Meter and by x-ray diffraction was chosen to be copper. There were several reasons for choosing this material, reasons relating to practicality and viability. First, copper is readily available in the forms required for the study. It is easy to obtain strips suitable for use in the I.S. Meter, and the disks needed for x-ray analysis could be made from standard 1 ¼" dia.

copper rods. Additionally, copper is one of the metals most commonly used as a substrate for electroplating and electroforming processes and therefore the choice is also practical in the application of the knowledge that would be obtained.

2.3 *Improved Modeling*

Traditionally, mathematical models used to calculate deposit stress have been developed using various differential methods. The resulting formulae attempt to provide a value for the "average" stress through the deposit thickness, using the net deflection that occurs after plating is completed. While not being entirely accurate in the purest mathematical sense, there is an inherent advantage to this type of model as the result is typically a closed-form equation relating overall deflection to a stress value.

There are several inadequacies with this kind of approach. First, the "average" stress reading obtained is rather difficult to interpret, and it does not truly define the state of stress in the deposit. Most models provide only a conversion of net strain in a single direction; some take into account the effects of lateral contraction. These readings are best interpreted as a scaling of the relative stress level in deposits from a given solution, not as the true state of stress in the deposit. Furthermore, it is not possible to use these models to obtain the instantaneous value of stress during the testing process; all that may be obtained is the average value throughout the entire deposited thickness.

For these reasons, a new approach in modeling the plating/deflection phenomenon was taken. Instead of viewing the process as continuous and smooth in its behavior, it was broken into a sequence of many discrete steps. Each of these steps is analyzed individually, and the result is a discretized numerical model that can be used to determine both average stress through the deposit and instantaneous stress in each layer.

The development of this technique is fairly straightforward. Before the test begins, the system consists of the substrate material only, with given properties (length, width, thickness, elastic modulus, and Poisson's ratio). The following figure details the substrate/deposit system. The term 'Δh' represents the thickness a differential layer of the deposit created on one side of the substrate, such that a total of '$2\Delta h$' is applied during each incremental step. All other terms are defined below. For the sake of simplicity, both the substrate material and the deposit material are assumed to have equivalent Poisson's ratios. Terms with the 'o' subscript denote initial properties of the strip.

Figure 12: Numerical Model

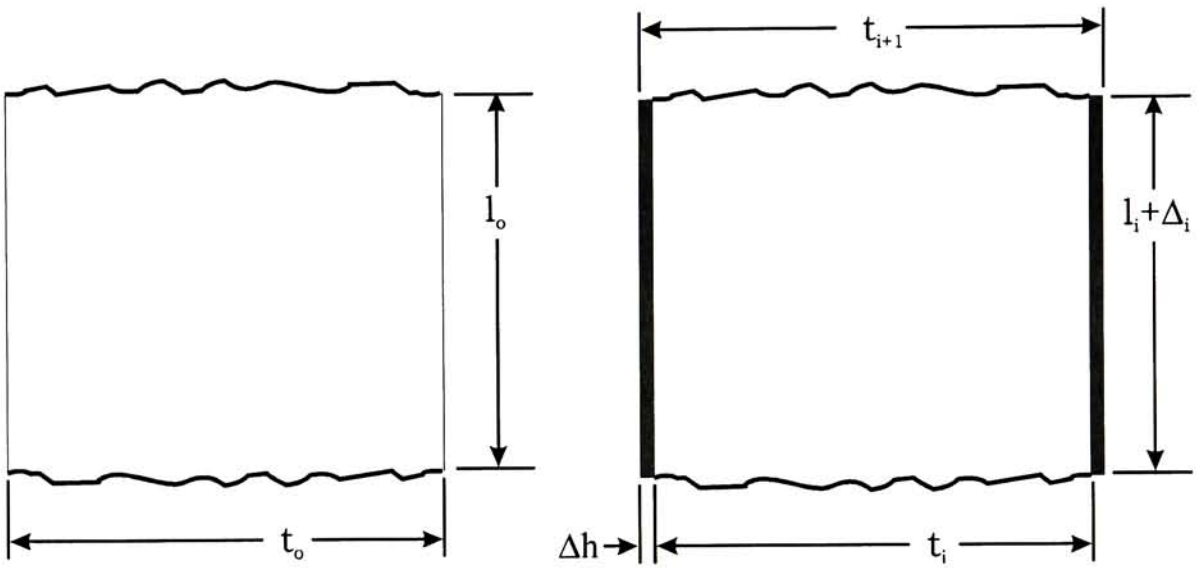

$$t_o = t_s$$

$$l_o = l_s$$

$$\tilde{E}_o = \frac{E_s}{\left(1-\upsilon_f\right)}$$

$$\tilde{E}_f = \frac{E_f}{\left(1-\upsilon_f\right)}$$

After one layer is deposited the following formula is used to calculate its equivalent stress, so long as deflection as a function of deposit thickness is known in closed form.

$$\sigma_o = \frac{-\Delta_o}{2 t_o l_o}\left(\tilde{E}_o t_o + 2 \tilde{E}_f \Delta h \right)$$

This formula is essentially identical to the one used in the model by Popereka, with one key exception. Since this equation is applied at the differential level, the need to assume that $d\Delta/dt$ is equal to Δ/t_f is eliminated. This represents a key improvement in the accuracy of the technique.

Since the system now consists of a "sandwich" (the substrate with deposited material on each side), it is possible to determine its new properties. As the second layer is deposited, the sandwich properties are used in the stress calculation and while these properties are again recalculated for the next iteration. This repeats throughout the extent of the test. Calculations are as follows:

Equation 5: Iterative Length Calculation

$$\boxed{l_{i+1} = l_i + \Delta_i}$$

l:	Substrate length
Δ:	Incremental Change in Substrate Length

Equation 6: Iterative Thickness Calculation

$$t_{i+1} = t_i + 2\Delta h$$

t:	Substrate Thickness
Δh:	Incremental Change in Deposit Thickness

Equation 7: Iterative Equivalent Elastic Modulus Calculation

$$\tilde{E}_{avg,i+1} = \frac{\tilde{E}_{avg,i}\, t_i + 2\,\tilde{E}_f\, \Delta h}{t_i + 2\Delta h}$$

E_f:	Deposit elastic modulus
Δh:	Incremental Change in Deposit Thickness
t:	Substrate Thickness

Equation 8: Iterative Instantaneous Stress Calculation

$$\sigma_i = \frac{-\Delta_i}{2 t_i l_i}\left(\tilde{E}_{avg,i}\, t_i + 2\,\tilde{E}_f \Delta h \right)$$

σ_i:	Instantaneous Deposit Stress Level
Δ:	Incremental Change in Substrate Length
t:	Substrate Thickness
l:	Substrate Length
E:	Substrate Elastic Modulus

The previous equations are used to determine the instantaneous value of stress for each incremental amount of material deposited. To calculate the average stress in the deposit, the following formula was used:

Equation 9: Average Stress Calculation

$$\sigma_{avg} = \frac{1}{n}\sum_{i=1}^{n}\sigma_i$$

σ_i:	Instantaneous Deposit Stress Level

In order to apply this model to actual test data some additional work is required. The data acquired from the tests were in the form of a list of deposit thickness values with a corresponding list of measured deflection values. These numbers had to be converted to a formula where deflection could be calculated as a function of deposit thickness, and this was accomplished numerically using the best-fit technique in Microsoft Excel. Verification of the fit was in the form of a least-squares fit and a subsequent comparison of the results. All data were fit to a second-order polynomial, as any higher order polynomial resulted in unrealistic inflection points in the instantaneous stress data. These inflection points had little bearing on the overall average stress calculated. All I.S. Meter test data were fitted in such a manner for each method of analysis.

The primary advantage of this technique is the elimination of the assumption that the substrate length will change at a constant rate throughout the entire plating process (i.e. assuming that $d\Delta/dt$ is equivalent to Δ/t). Because this equation is applied more frequently in the numerical model, at an order of magnitude closer to the differential level, such an assumption becomes much more viable.

In order to compare the results obtained with this model with those obtained from Equations 3 and 4, Figure 13 has been supplied. In this chart two new data sets have been added - instantaneous stress as calculated by the numerical model and the 'average' stress as calculated by the numerical model. Each point on the average stress curve is the average of all instantaneous stress values from the onset of deposition to that point. The average deposit stress, calculated in this manner, is useful if it is desired to compare the results of this formula with those of the previous two.

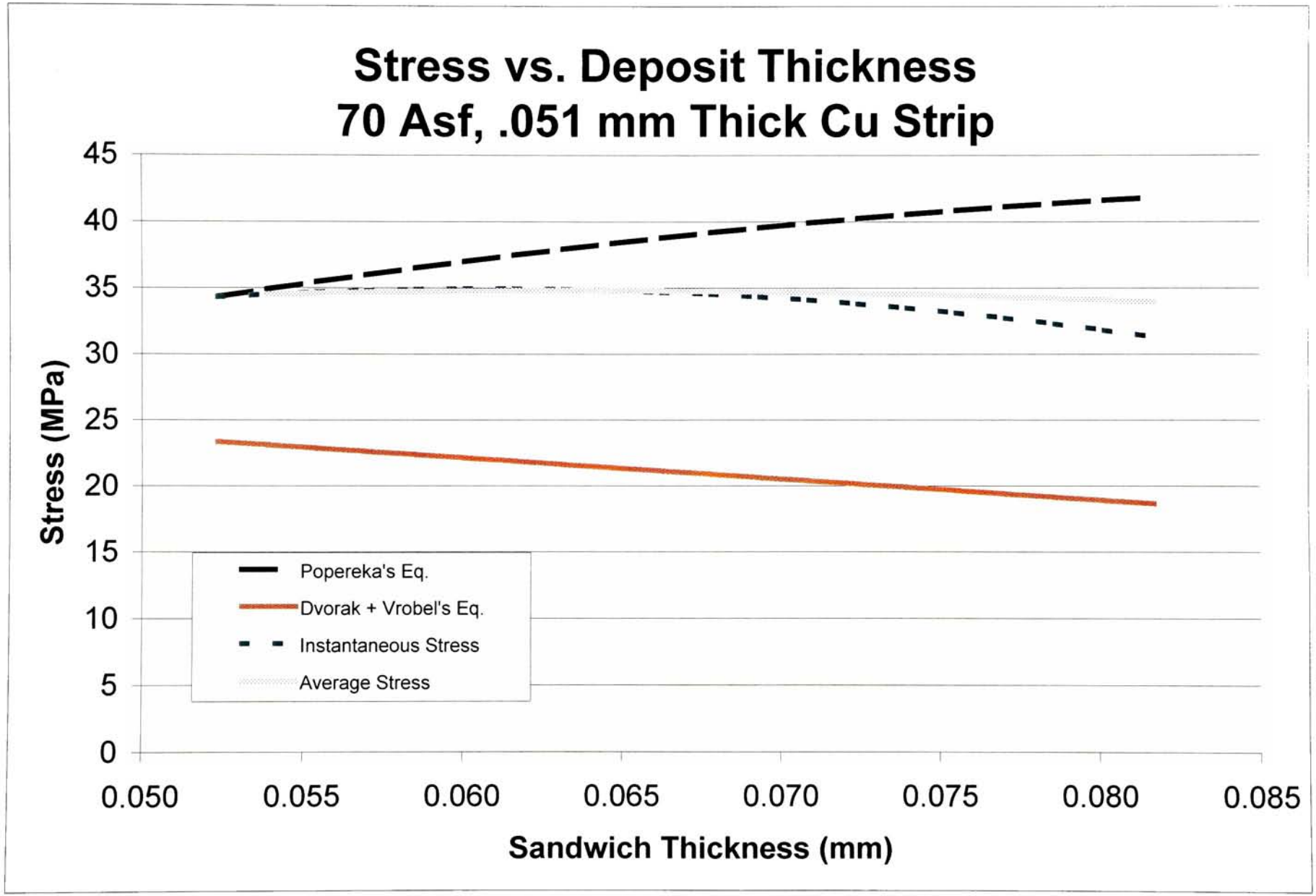

Figure 13: I.S. Meter Data with Traditional and Numerical Analysis

As stated previously, neither of the two traditional formulae yield realistic stress versus deposit thickness patterns for this set of data. Popereka's formula results in a curve that rises with deposit thickness while Dvorak and Vrobel's formula gives a curve that drops off as thickness increases.

The numerical model does however provide a realistic pattern in the stress versus deposit thickness curve. For the first half of deposition, instantaneous and average stress values are essentially the same. This results in a curve that is nearly flat, especially when viewed in contrast with the two previously discussed curves. After this time, instantaneous stress begins to fall off slightly; however, the magnitude of the change is much less than that exhibited in either of the other two curves. Physically, there may well be a gradual lessening of stress as deposit thickness increases; however, this is not necessarily the case. All of these formulae are based on assumptions that the deposit thickness is small in comparison to the substrate thickness and they are simply not accurate as deposit thickness increases to the point where it is a significant percentage of substrate thickness (as it does in this case, where the substrate thickness is 0.052 mm).

Ch. 3 Stress Analysis with X-Ray Diffraction

3.1 X-Ray Background

When x-ray radiation is incident upon the surface of a crystalline substance the regular arrangement of atoms will allow diffraction at only one particular angle, as shown in the following figure. This angle is that at which constructive interference occurs between diffracted rays, the so-called "Bragg angle" given by Bragg's Law:

Equation 10: Bragg's Law

$$\lambda = 2d\sin(\theta)$$

λ:	Wavelength of X-radiation (m)
d:	Lattice Spacing (m)
θ:	Angle of Incidence (rad)

Figure 14: X-ray Diffraction by a Crystal Lattice

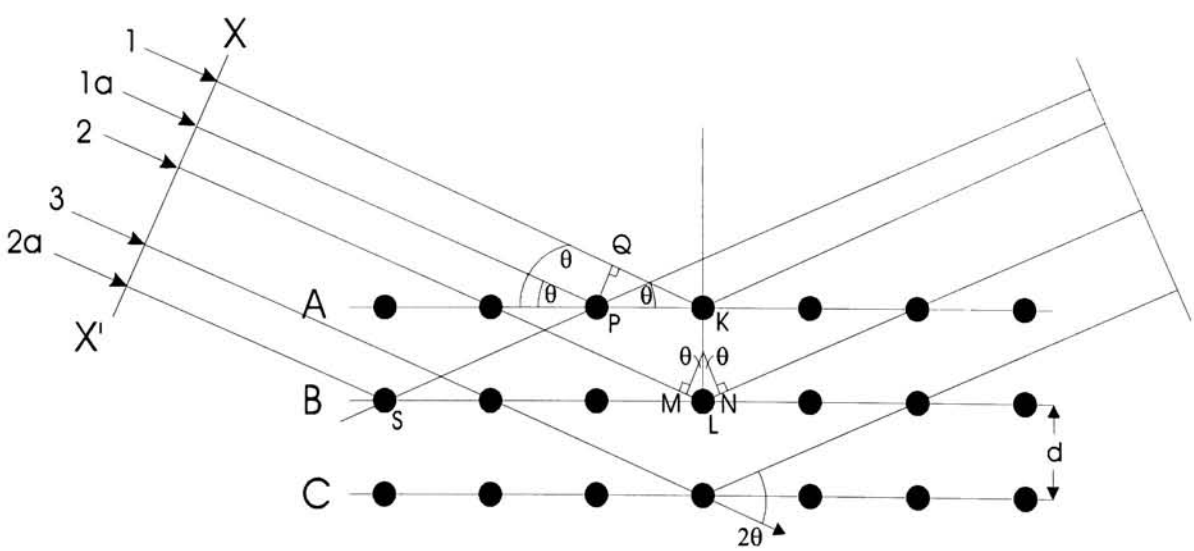

The angle θ is a function of the interplanar spacing, d, and the wavelength of the incident radiation. Knowing this, it is possible to determine the parameter d of a crystal lattice by exposing its surface to x-rays through a wide range of θ values and measuring the angular locations at which diffraction occurs. So long as the wavelength of the incident radiation is known, it is possible to calculate d using Equation 10. This phenomenon is known as x-ray diffraction.

Generally, x-ray diffraction measurements are performed by an x-ray diffractometer, an instrument designed specifically to locate the angles at which diffraction occurs. These instruments consist of a cathode ray tube to provide the x-rays, a detector to record diffracted photons, and a stage upon which the sample to be irradiated is held. Typically, the cathode ray tube remains stationary, while the sample is rotated through a maximum possible range of 90 degrees. The angle between the surface and the x-rays is θ, and to record diffraction the detector is moved synchronously with the surface but at twice the angular velocity. In this way when the surface is rotated by θ with respect to the source, the detector will be rotated by 2θ. The output of a diffractometer is a plot of intensity values versus the corresponding 2θ values at which they occurred.

The range of measurements possible is approximately $20^{o} < 2\theta < 160^{o}$ because making very large or high angle measurements would require that the source and the detector occupy the same space and at low angles there exists the risk of

exposing the detector to direct radiation rather than diffracted radiation.

In a perfectly monocrystalline material more than one peak may be observed in the plot of intensity versus 2θ, depending on the orientation of the sample. This is due to the fact that diffraction may occur along planes having regularly spaced atoms, and many of these planes can yield a significant amount of diffraction (the closer the atoms are to one another in these planes the more diffraction that will occur). However, because not all crystal planes will be oriented in such a manner as to allow diffraction to occur, it is never possible to observe all peaks with a single scan at a given sample orientation.

When a polycrystalline material is examined in an x-ray diffractometer the results are quite different. Because metals are composed of numerous grains, whose orientation is generally random, many more peaks are noticeable for a given scan. Theoretically, if the three-dimensional grain orientation is perfectly random throughout the sample, peaks will occur for all of the d values corresponding to all of the planes for which diffraction can happen. In practice however, this is not generally the case. Many planes have such low amounts of diffracted radiation that they can not be separated from the noise in the data, and any preferred orientation of the grains in the sample will emphasize the relative intensity of some peaks while diminishing that of others. In some cases, preferred orientation can lead to the absence of significant peaks altogether.

Figure 15: Stress Tensor

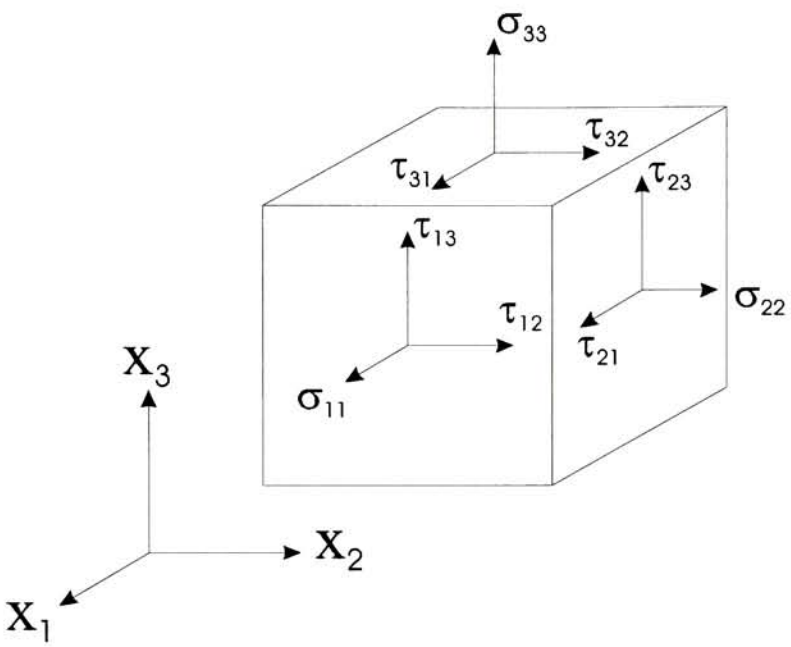

Stress Tensor σ_{ij}

$$\sigma_{ij} = \begin{bmatrix} \sigma_{11} & \tau_{12} & \tau_{13} \\ \tau_{21} & \sigma_{22} & \tau_{23} \\ \tau_{31} & \tau_{32} & \sigma_{33} \end{bmatrix}$$

Principal Stresses

$$\hat{\sigma}_{ii} = \begin{bmatrix} \sigma_{xx} & 0 & 0 \\ 0 & \sigma_{yy} & 0 \\ 0 & 0 & \sigma_{zz} \end{bmatrix}$$

3.2 Calculation of Stress Field

Figure 15 is intended to clarify naming conventions for elements of the three-dimensional volumetric element and the stress tensor σ_{ij}.

For the purpose of using x-ray diffraction several key assumptions may be made. Most notably, since all measurements are made at the surface of the sample, the stress component in the direction perpendicular to the surface (σ_{33}) must be equal to zero. Realistically this is not entirely true due to the fact that diffraction occurs not at the surface, but inside a penetration depth of about 25 μm. For the purpose of this research, this assumption is acceptable primarily because x-ray measurements

will be compared to a measurement technique that is concerned with the two-dimensional state of stress parallel to the sample surface and therefore any stresses in the z-direction will have minimal impact.

Measurements of stress by x-ray diffraction are based upon the ability to measure the interplanar spacing of atom layers. The most basic measurement possible therefore is to measure the spacing of planes parallel to the surface, knowing that any strain in this direction is due to contraction by the Poisson effect alone since σ_{33} has been assumed to be equal to zero. This would allow the calculation of the sum of the principal stresses acting in the plane of the sample surface.

$$\frac{d_n - d_o}{d_o} = \frac{-\upsilon}{E(\sigma_1 + \sigma_2)}$$

In this case, d_n represents the actual spacing measured perpendicular to the surface, while d_o is the value for the unstrained condition. Unfortunately, this method would require knowing the unstressed value d_o. This value may change depending on the impurities in the deposit [8, p455], so any listed value for the parameter may not be accurate.

In order to begin to develop a model that will allow measurement of both principal stresses and their directions it is first necessary to define a coordinate system that will describe the orientation of the sample relative to the plane of

measurement by the x-ray diffractometer. This coordinate system will consist of two angles, ϕ and ψ. The first angle ϕ defines the rotation of the sample about its center, the axis being the surface perpendicular, which is referenced from the vertical. The second angle ψ defines the rotation of the sample about its own vertical axis, which is referenced from a zero point where the surface normal will be parallel to the incident and diffraction x-rays when θ is equal to zero. This is demonstrated in Figure 16, where $\underline{S}$ represents the sample coordinate system (ϕ being a rotation about $\underline{S}_3$) and $\underline{L}$ represents the coordinate system of the x-ray diffractometer ($-\underline{L}_3$ being the direction of incident radiation).

Figure 16: Sample Coordinate System

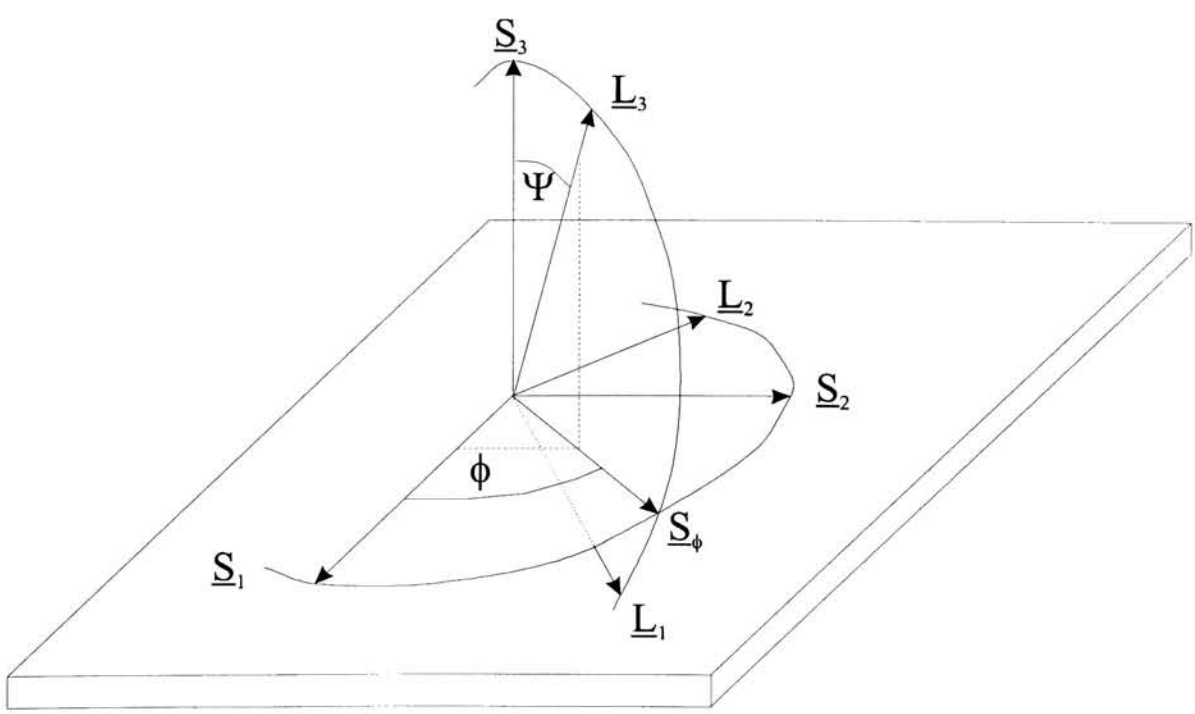

Figure 17: Measurement of d_ψ

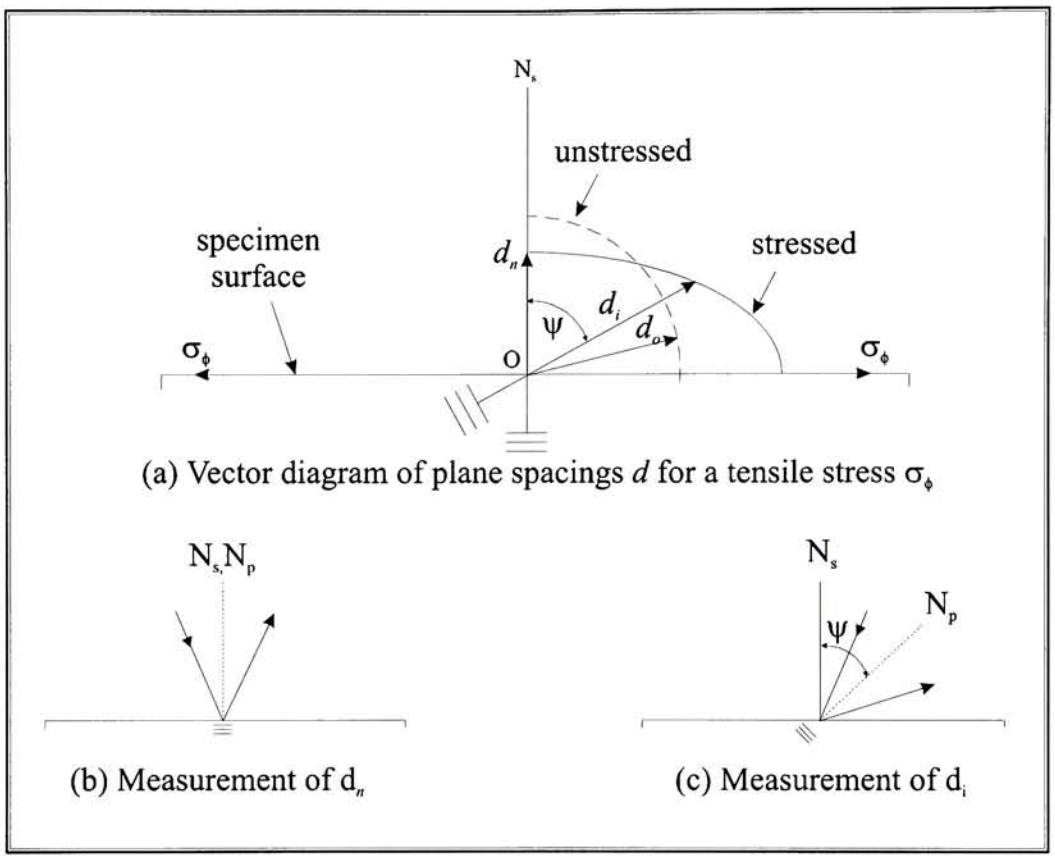

Figure 17 details the measurement of strain, both normal to the surface and at the angle ψ. In each case the diffractive planes are designated by a series of three parallel lines.

The projection of the strain tensor ε_{ij} onto a unit vector in the direction of L_3 represents the strain that will be measured by x-ray diffraction when the surface is oriented at ϕ and ψ. This can be represented by the following equation:

$$\varepsilon'_{33} = a_{3k} a_{3l} \varepsilon_{kl}$$

Substituting for the directional cosine matrix a_{ik} of the surface normal yields:

$$\varepsilon_{33}' = \varepsilon_{11}\cos^2\phi\sin^2\psi + \varepsilon_{12}\sin 2\phi\sin^2\psi$$
$$+\varepsilon_{22}\sin^2\phi\sin^2\psi + \varepsilon_{33}\cos^2\psi$$
$$\varepsilon_{13}\cos\phi\sin 2\psi + \varepsilon_{23}\sin\phi\sin 2\psi$$

In a polycrystalline material it is possible to obtain a diffracted beam at any Ψ tilt, and it is therefore possible to calculate ε'_{33} at any Ψ tilt. Examining $d_{\phi\psi}$ vs. $\sin^2\psi$ data, there are three basic patterns of behavior that may occur. These are detailed in Figure 18.

Figure 18: Behavior of $d_{\phi\psi}$ vs. $\sin^2\psi$

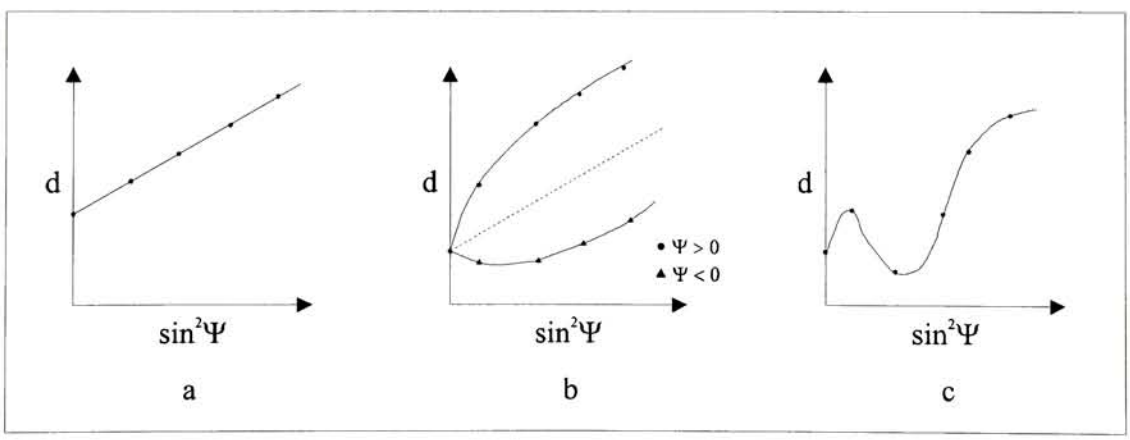

Figure 18a depicts "regular" $d_{\phi\psi}$ vs. $\sin^2\psi$ behavior, where a linear relationship exists because ε_{12} and ε_{23} are equal to zero. Figure 18b also depicts "regular" behavior, but because one or both of the components ε_{12} and ε_{23} are

non-zero, the d values measured at plus and minus ψ locations will be different. This effect is due to the association of $\sin 2\psi$ with these terms in the previous equation, and is know as "ψ-splitting". Finally, Figure 18c depicts irregular oscillatory behavior that cannot be analyzed with the previous equation [9, p119].

From general elasticity theory it can be shown that the strain on the specific crystal planes measured when the surface is oriented at ϕ and ψ is

Equation 11: Strain at Angles Φ and Ψ

$$\boxed{\varepsilon_{\Psi,\Phi} = \frac{1}{E}\left(\sigma_{\Phi}(1+\upsilon)\sin^2(\Psi) - \upsilon(\sigma_1+\sigma_2)\right)}$$

Note that when $\psi = 0$ the $\sin^2(\Psi)$ term disappears and this equation reverts to the following.

$$\frac{d_{\psi=0} - d_o}{d_o} = \frac{-\upsilon}{E(\sigma_1+\sigma_2)}$$

When two measurements of d are made, holding ϕ constant but varying ψ from 0 to some arbitrary value the following expression is achieved by subtracting the strain values measured in each case:

$$\varepsilon_{\Psi,\Phi} - \varepsilon_{3,\Phi} = \frac{1}{E}\sigma_{\Phi}(1+\upsilon)\sin^2(\Psi)$$

Expressing the strains in terms of plane spacing the formula becomes

$$\frac{(d_{\Psi} - d_o)}{d_o} - \frac{(d_3 - d_o)}{d_o} = \frac{(d_{\Psi} - d_3)}{d_o} = \frac{1}{E}\sigma_{\Phi}(1+\upsilon)\sin^2(\Psi)$$

In this equation d_3 is used to denote the lattice spacing of the planes normal to the surface, i.e. $d_3 = d_{\psi=o}$. Once again, this formulation requires knowing the unstressed plane spacing d_o. However, since d_o, d_{ψ} and d_3 are very nearly equal to one another, and the value d_{ψ}-d_3 is very small when compared to d_o, very little error is introduced when the value of d_3 is used in place of d_o for calculations. This yields the final version of this equation

$$\frac{(d_{\Psi} - d_3)}{d_3} = \frac{1}{E}\sigma_{\phi}(1+\upsilon)\sin^2(\Psi)$$

With this information it is possible to calculate the properties of the two-dimensional stress field acting on the surface of the sample by measuring $(d_\psi - d_3)/d_3$ versus $\sin^2(\psi)$ for three different ϕ locations. These locations are designated as ϕ, $\phi + \alpha$, and $\phi - \alpha$. When $\sigma_\phi, \sigma_{\phi+\alpha}$, and $\sigma_{\phi-\alpha}$ have been measured, the basic equations of Mohr's circle are used to determine σ_1, σ_2 and ϕ_1 (the principal angle at which σ_1 occurs) as follows [10, p337]. These equations were developed with $\alpha = 60$ degrees, which was the case in the research as well.

$$\sigma_{1,2} = \frac{E}{3}\left[\frac{\varepsilon_{\phi-60} + \varepsilon_{\phi+60} + \varepsilon_\phi}{1-\upsilon} \pm \frac{\sqrt{2}}{1+\upsilon}\sqrt{(\varepsilon_{\phi-60} - \varepsilon_{\phi+60})^2 + (\varepsilon_{\phi-60} - \varepsilon_\phi)^2 + (\varepsilon_\phi + \varepsilon_{\phi+60})^2}\right]$$

$$\tan(2\phi_1) = \frac{\sqrt{3}(\varepsilon_\phi - \varepsilon_{\phi+60})}{2\varepsilon_{\phi-60} - (\varepsilon_\phi + \varepsilon_{\phi+60})}$$

Because measurements were taken at orientations of 0, 60, and 120 degrees, these equations require some modification. To make them compatible, ϕ must be set to 60 degrees as in Equations 12 and 13 as follows.

Equation 12: Principal Stress Calculation

$$\sigma_{1,2} = \frac{E}{3}\left[\frac{\varepsilon_0 + \varepsilon_{120} + \varepsilon_{60}}{1-\upsilon} \pm \frac{\sqrt{2}}{1+\upsilon}\sqrt{(\varepsilon_0 - \varepsilon_{120})^2 + (\varepsilon_0 - \varepsilon_{60})^2 + (\varepsilon_{60} + \varepsilon_{120})^2}\right]$$

Equation 13: Principal Angle Calculation

$$\tan(2\phi_1) = \frac{\sqrt{3}(\varepsilon_{60} - \varepsilon_{120})}{2\varepsilon_0 - (\varepsilon_{60} + \varepsilon_{120})}$$

3.3 Specimen Specifics

In preparing samples for x-ray analysis, efforts were made to duplicate the conditions of testing in the I.S. Meter. Copper was used as a substrate, although thickness was increased so as to minimize the relieving of internal stresses as plating occurred.

Samples were plated in roughly the same position and orientation with the sides of the disks perpendicular to the anode. The samples were made concurrently with the I.S. Meter tests, although sufficiently far enough away from the instrument to assure they had no effect on one another (either electrochemical or fluid-flow related). Finally, plastic tape was placed around the circumference of the disks in order to provide shielding and to yield a constant deposit thickness across the surface. Since the edges of the disks were masked in this manner, plating occurred only on the flat surfaces and the effects of changes in surface geometry previously discussed were minimized.

The size of the samples was dictated by the chamber of the x-ray diffractometer and by the fact that samples must be scanned at various Ψ angles. Obviously, the samples needed to be disk-shaped to allow the Ψ rotation, and the maximum diameter that could feasibly be used was limited. This created the need for a compact mounting device that would allow rotation of the specimen while fitting into the chamber. Since such a mounting device was not available, one had to be

created by the author. The fixture, designed and built to fill this purpose, is detailed in Figure 19.

Figure 19: Specimen Holder for X-ray Diffractometer

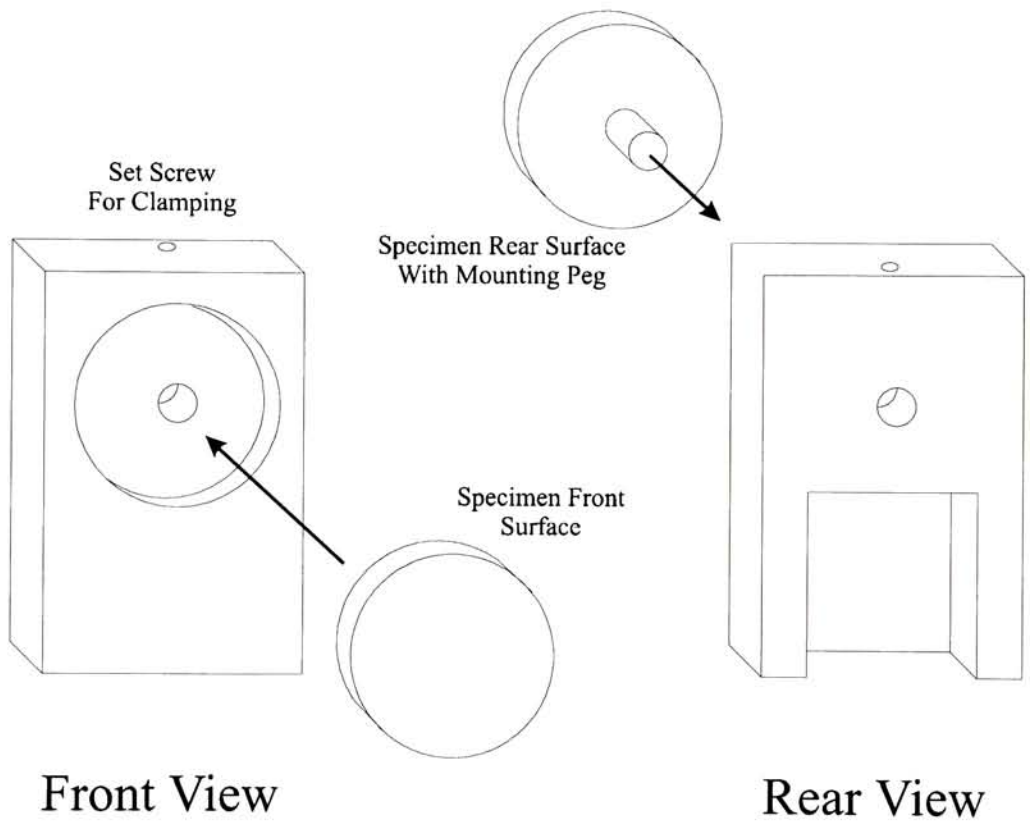

The mounting device was made from polycarbonate, and its size was approximately 2" high by 1.5" wide by .3" thick. An alignment slot on the bottom of the fixture was installed to assure repeatable positioning from sample to sample, both in angle and position relative to the x-ray source. In order to mount a copper disk in the fixture it was necessary to glue a PVC cylinder to its back and insert the pair into

the mounting hole. The entire assembly was then placed facedown onto a flat surface and the set screw was tightened to lock the disk in position.

This setup provided several features necessary in this investigation. First, no external forces were applied to the disk during the testing process, as any applied force would have some effect on the state of stress in the nickel-copper-nickel sandwich. Additionally, the sample could be easily rotated between scans simply by loosening the set screw and remounting the disk. Unfortunately, mounting a specimen in this manner introduces error in its alignment. To assure that these errors were not significant, sample displacement scans were made using both the sample holder and larger specimens held in the traditional manner.

3.4 Specifics of X-ray tests

All specimens were examined with the same parameters on the x-ray diffraction machine. The tube was operated at a current of 35 mA at 40 kV, and no monochromator was used. Because the samples were covered with the nickel deposits, it was not necessary to utilize a nickel filter. Step scans were used for all measurements, taking intensity readings every 0.05 degrees over a range of 1 degree for a total duration of 60 seconds.

Data exported from the measurement software was in the form of intensity values measured at each angular position. This was imported into Microsoft Excel, where it was analyzed. The corrected intensities were plotted against 2θ, and the

"Solver" utility, a tool capable of solving multivariate equations by minimizing least square values, was used to determine the peak location based on a least squares parabolic fit.

Ch. 4 Results and Conclusion

4.1 Plating Conditions and Sample Preparation

In order to compare the results of traditional stress measurement techniques with those of x-ray measurements, it was necessary to prepare samples representing a wide range of internal stress values. Using a given electroplating bath, one of the most effective means of altering deposit stress was by varying the current density at which plating occurred. In general, stress and current density are directly related. Specifically, in the nickel sulfamate baths used to prepare samples for this research, high current density plating results in highly stressed deposits while plating at lower current densities yields lower deposit stress. For current density, units of Amperes per square foot were used, as this is the standard for the electroplating industry (1 A/ft^2 = 0.108 A/dm^2). Furthermore, because nearly every physical and chemical property of the tank (temperature, pH, impurities present, etc.) has an effect on deposit stress, the overall 'state of stress' in a tank shifts continuously. These two factors allow one to obtain samples over the wide range of stress values desired.

In this study, pairs of samples for x-ray analysis were prepared under four different stress conditions, and a test was taken with the I.S. Meter at each of these conditions. Samples #1 and #2 were prepared in a compressively stressed bath under identical conditions, at a current density of 15 A/ft^2. This was intended to yield a very highly compressive deposit. Samples #3 and #4 were prepared in the same bath shortly afterward, but at a current density of 30 A/ft^2. In this case the deposit stress

should still have been compressive, but the magnitude of deposit stress should have been greatly diminished. Samples #5 and #6 were plated in a different bath, one in which low tensile stresses would occur at the same 30 A/ft^2 current density. Finally, samples #7 and #8 were prepared in the same bath as #5 and #6 but at a current density of 45 A/ft^2. Here the deposit should have had a highly tensile internal stress.

4.2 Results of I.S. Meter Testing

The following charts depict stress calculations made with the data taken by the I.S. Meter. Included are the results obtained when Popereka'a formula, Dvorak and Vrobel's formula, and the numerical model are used to calculate average stress values through the plating process (as well as instantaneous stress in the case of the numerical model).

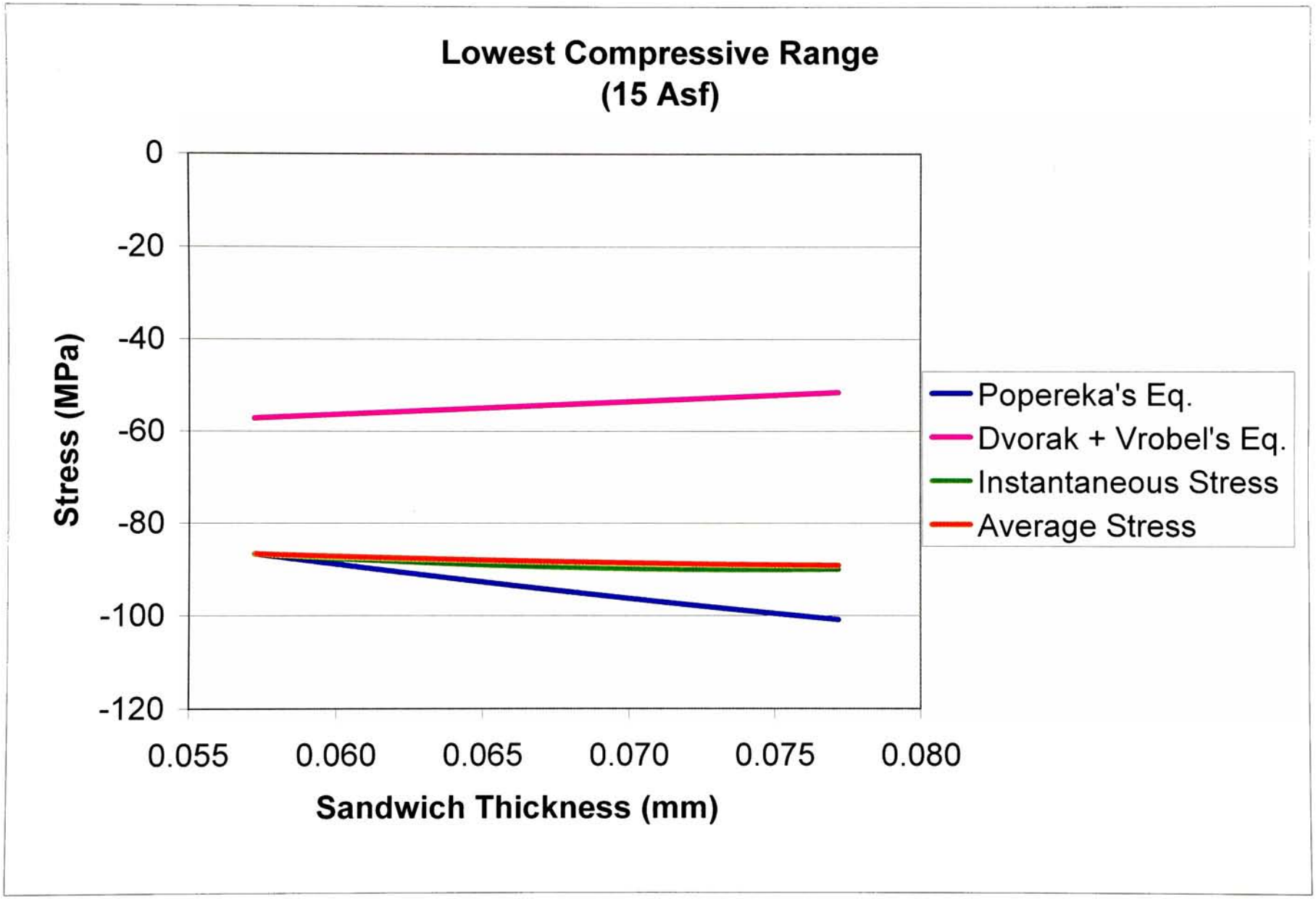

Figure 20: 15 Asf Lowest Compressive I.S. Meter Results

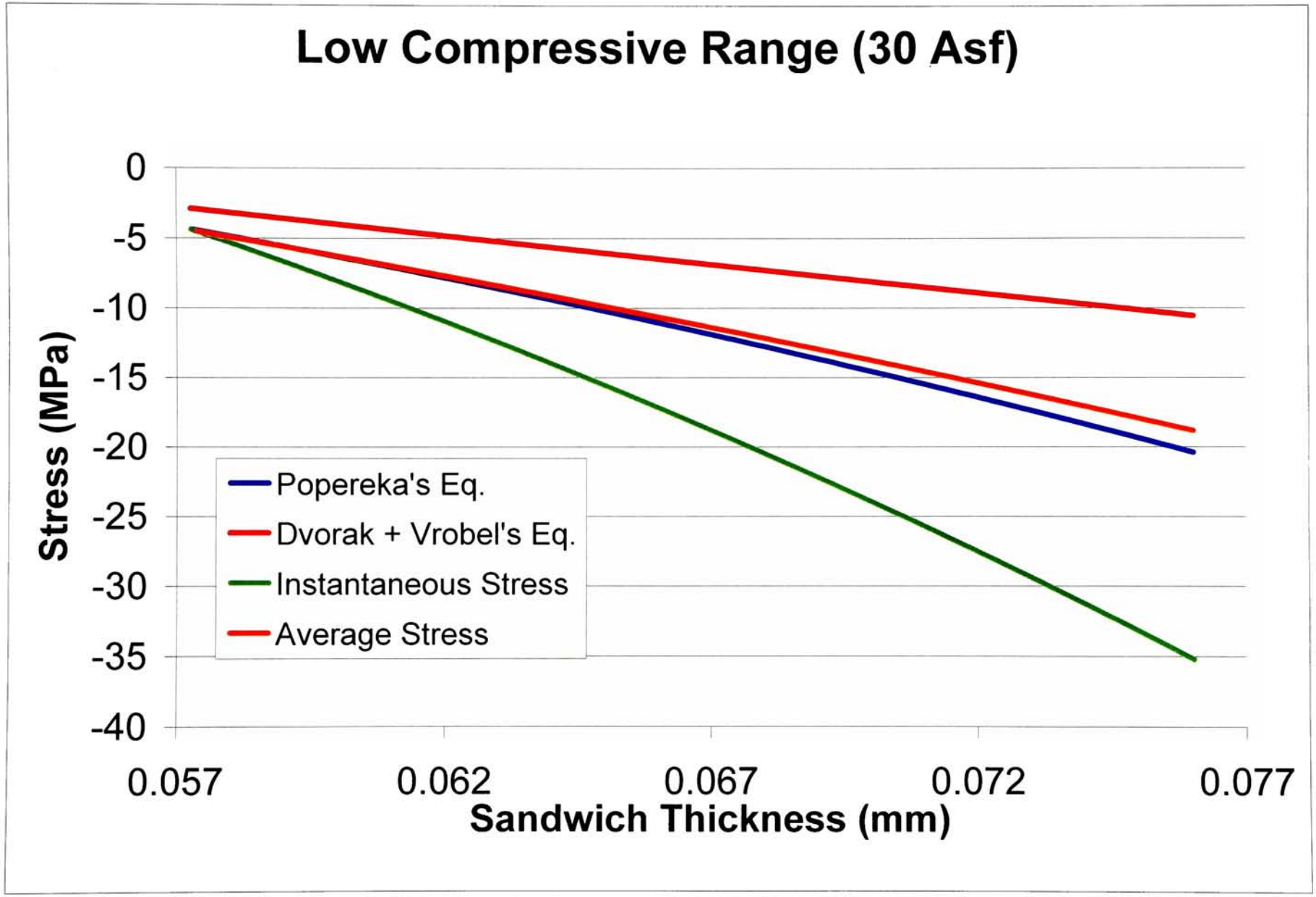

Sheet1 Chart 74

Figure 21: 30 Asf Low Compressive I.S. Meter Results

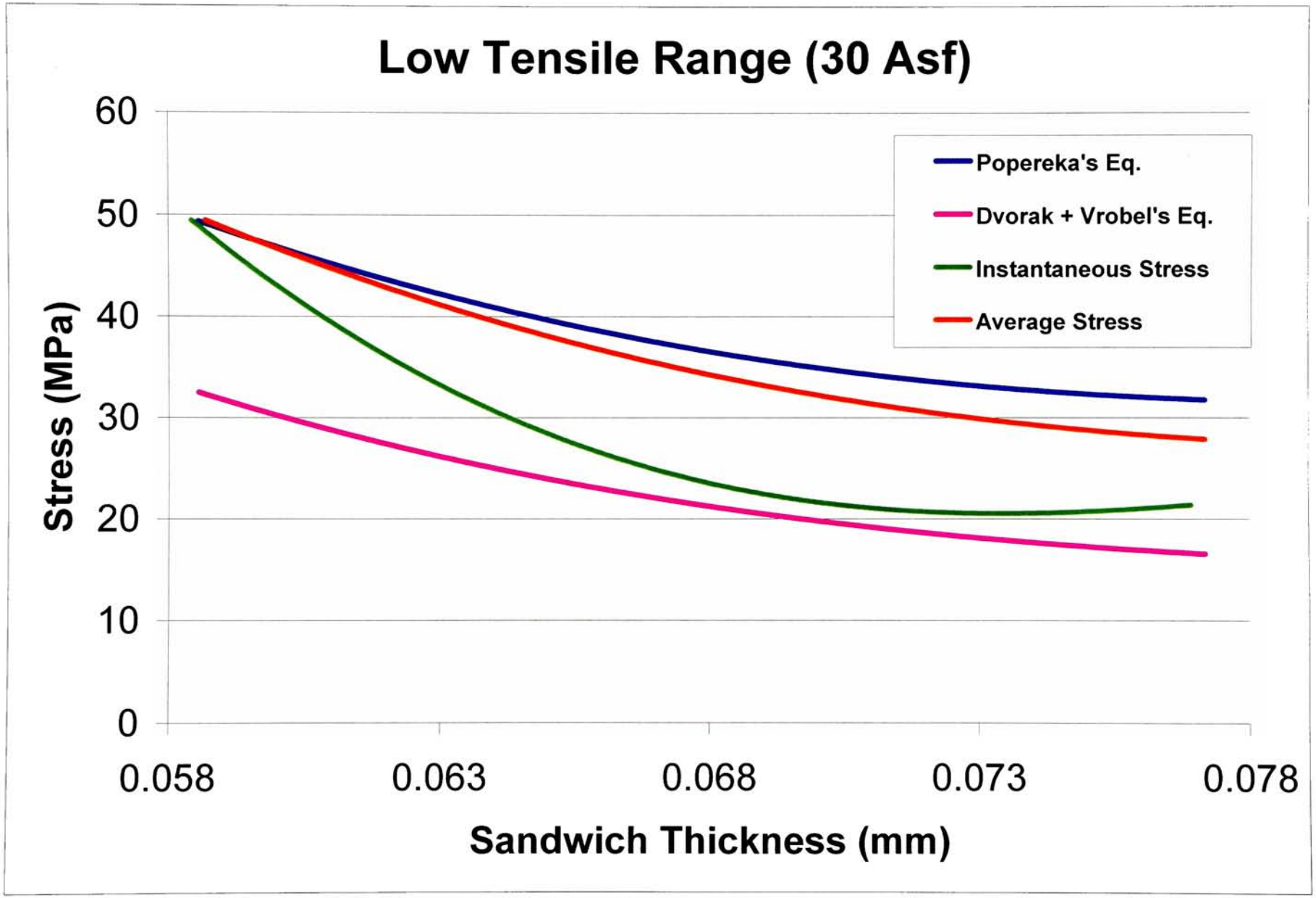

Figure 22: 30 Asf Low Tensile I.S. Meter Results

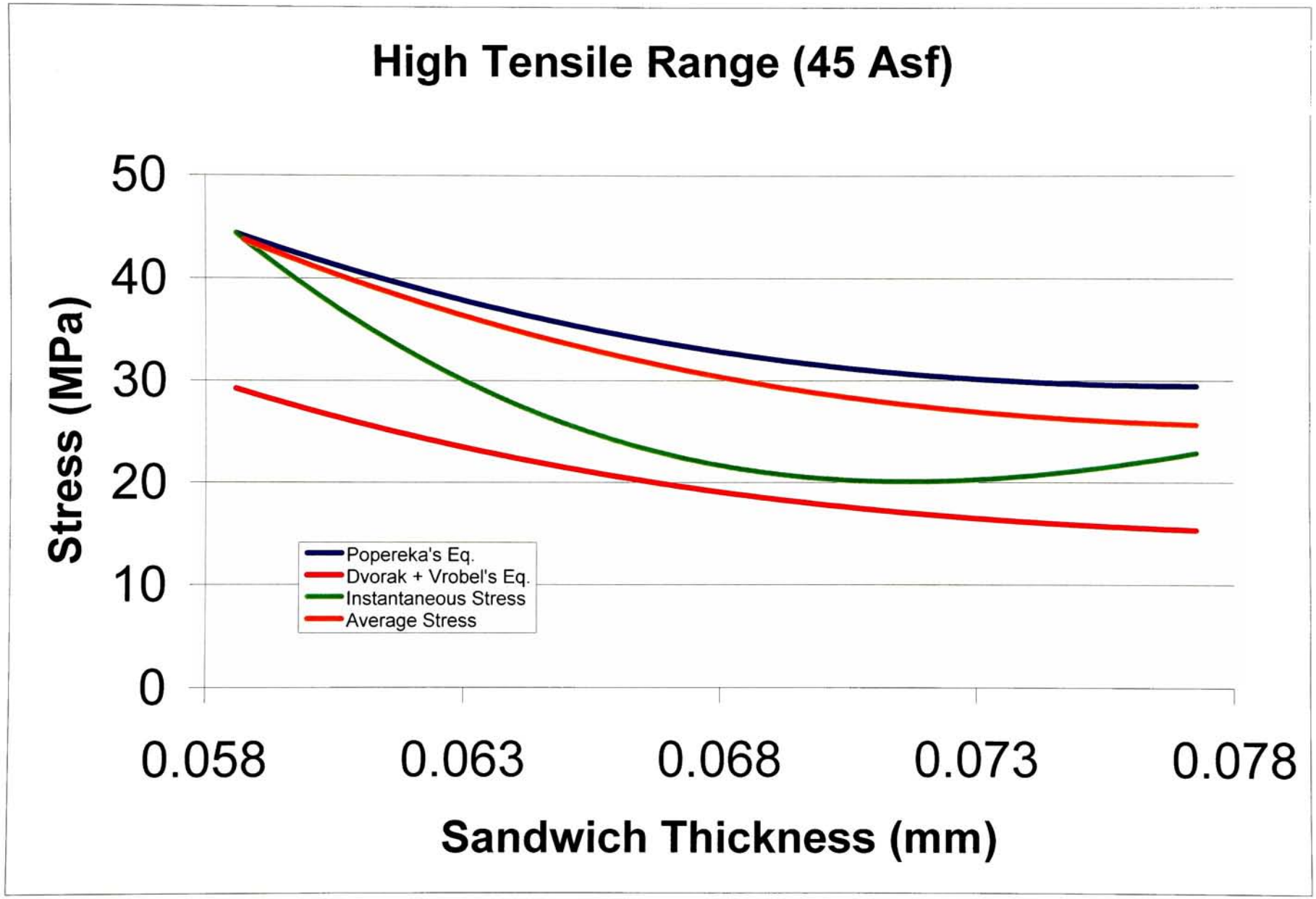

Figure 23: 45 Asf High Tensile I.S. Meter Results

Results from the tests taken at each of the four experimental conditions are displayed in the chart below; each value is in MPa. This chart gives values for the "average" stress occurring over the last 25% of deposition. This depth was chosen as it corresponds roughly to the depth at which only 50% of the x-rays will penetrate.

Figure 24: Summary of Stress Measurements from I.S. Meter Testing

Mathematical Model Used	Condition 1: 15 Asf High Compressive (MPa)	Condition 2: 30 Asf Low Compressive (MPa)	Condition 3: 30 Asf Low Tensile (MPa)	Condition 4: 45 Asf High Tensile (MPa)
Popereka	-99.30	-18.44	32.13	29.61
Dvorak & Vrobel	-52.24	-9.76	16.98	15.64
Numerical (Avg of Inst)	-90.07	-31.46	21.05	21.95
Numerical (Avg of Avg)	-88.96	-17.15	28.42	26.00

It is immediately apparent that according to these measurements there was very little change between the two samples that were supposedly plated at different levels of tensile stress. It may be assumed that these tests were taken at higher current densities where stress no longer varied but was essentially constant (see Figure 10). Otherwise, the remaining samples reflect the stress ranges that were initially desired. Additionally there is a strong correlation between the analysis done with Popereka's formula and the average stress as calculated by the numerical model.

4.3 *Results of X-Ray Testing*

Samples for x-ray analysis were prepared as described previously, except for the fact that the top of the back surface of each sample was marked. This was used as a reference for the $\phi = 0$ location, and it is from this line that the directions of the principal stresses measured are referenced.

Early in the research it was apparent that simply measuring a peak location at two values of ψ would not provide the precision desired. Although much previous work in this area relied simply on measurements at ψ angles of zero and forty-five degrees, several factors made this approach impractical. First, the stresses that were to be measured were only slightly above the error in measurement provided by the previous technique. Furthermore, microstresses were apparent in each of the samples analyzed. These microstresses cause the broadening of peaks, and they can also decrease the symmetry of a peak. Together these factors led to a significant loss of accuracy in determining the location of a given peak. To compensate for the above, several actions were taken. The 155-degree nickel peak was chosen as it was the closest observed peak to 180 degrees and because many of the other peaks simply disappeared for most ψ angles other than zero. This was evidence of a strong preferred orientation occurring in the deposits. Finally, measurements were taken over a wide range of ψ angles; -45, -40, -33, -27, -18, 0, 18, 27, 33, 40, and 45 degrees. These specific values were taken because d will theoretically vary linearly with $\sin^2(\psi)$, and these angles are approximately equally spaced in such a plot.

Note that because $\sin^2(\psi) = \sin^2(-\psi)$ there will be two peak locations measured at each $\sin^2(\psi)$ location, one from a rotation to $+\psi$ and the other from a rotation to $-\psi$.

When 2θ values of peak locations were taken at each of these ψ orientations, a best-fit line was determined. The intercept of this line was used to calculate the experimental value for d_3, while the value of d_ψ was determined by multiplying the slope by 0.5 (the value of $\sin^2[45]$), adding this to the intercept, and converting with Bragg's law.

Figures 25 through 32 depict peak location versus $\sin^2(\Psi)$ for the scans at Φ=0,60, and 120 degrees taken with each of the 8 samples prepared.

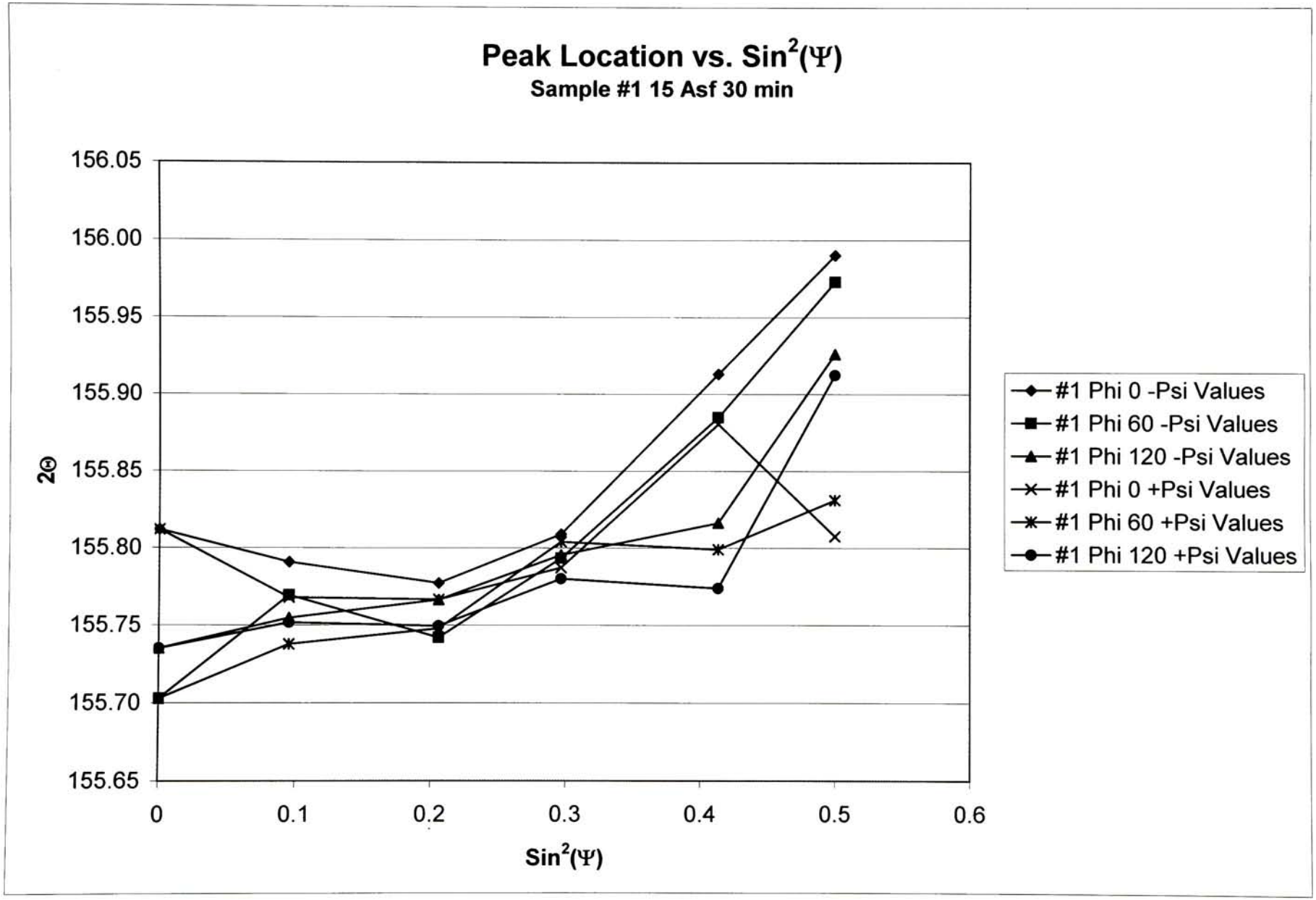

Figure 25: 15 Asf Lowest Compressive XRD Results (1)

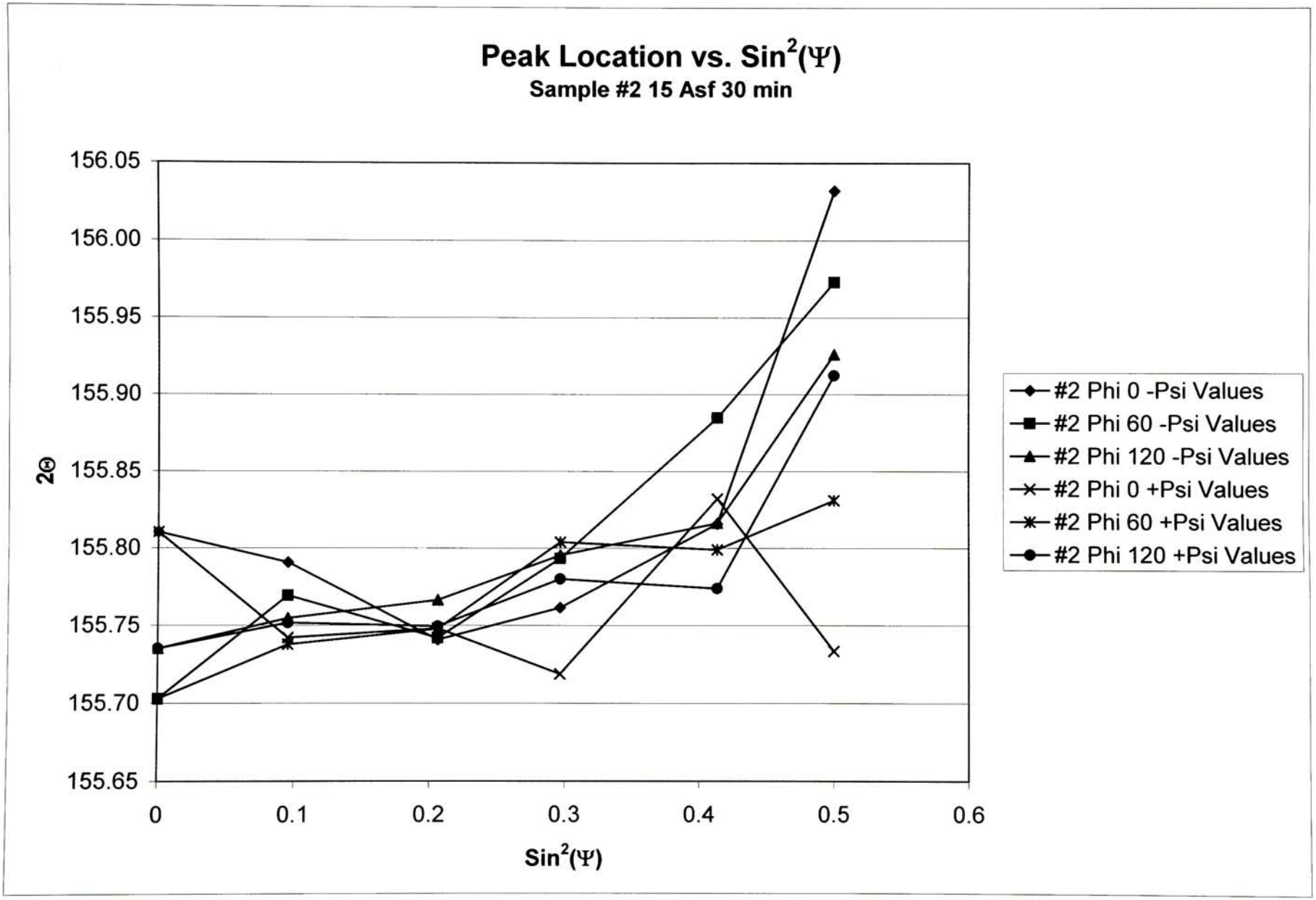

Figure 26: 15 Asf Lowest Compressive XRD Results (2)

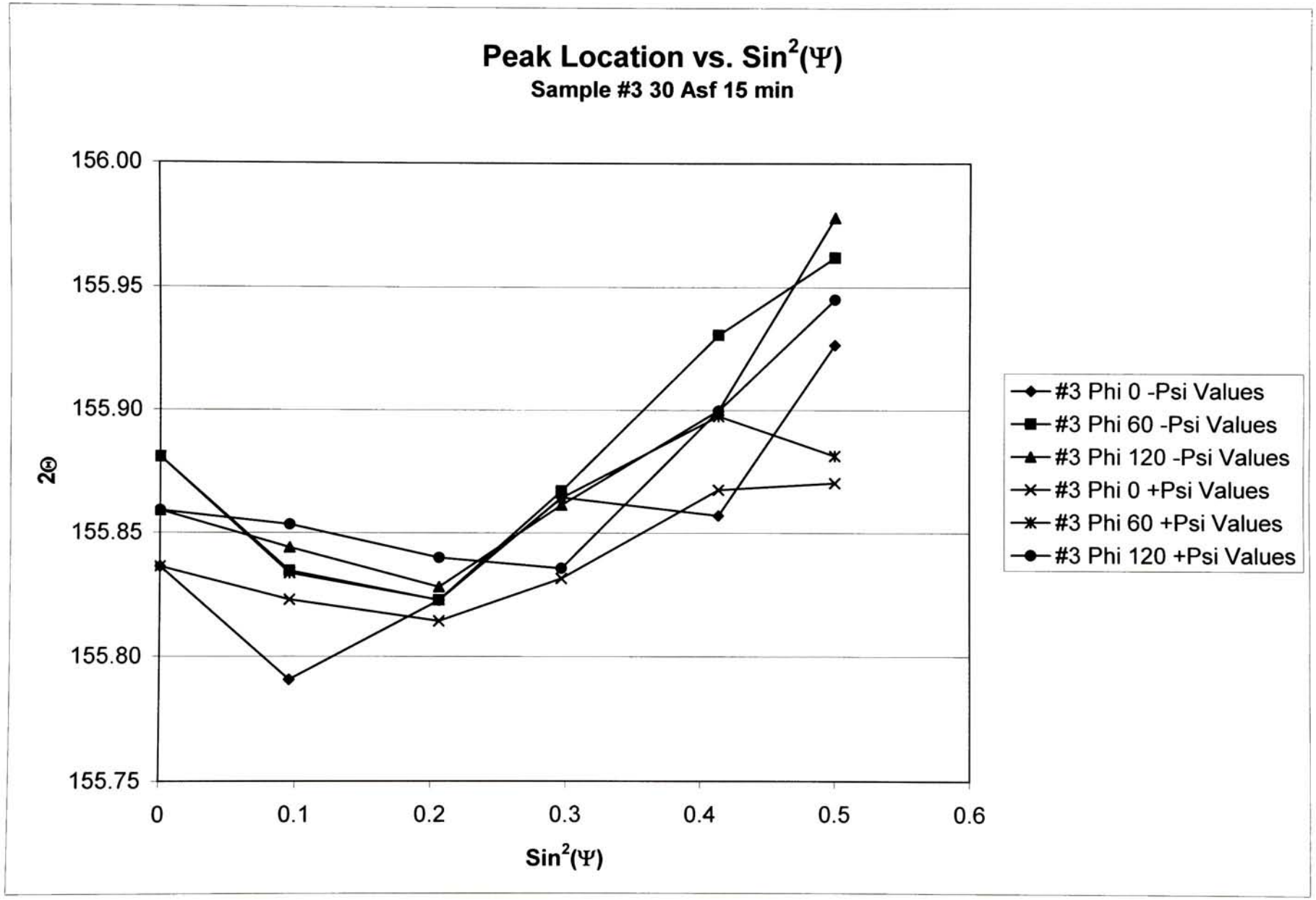

Figure 27: 30 Asf Low Compressive XRD Results (3)

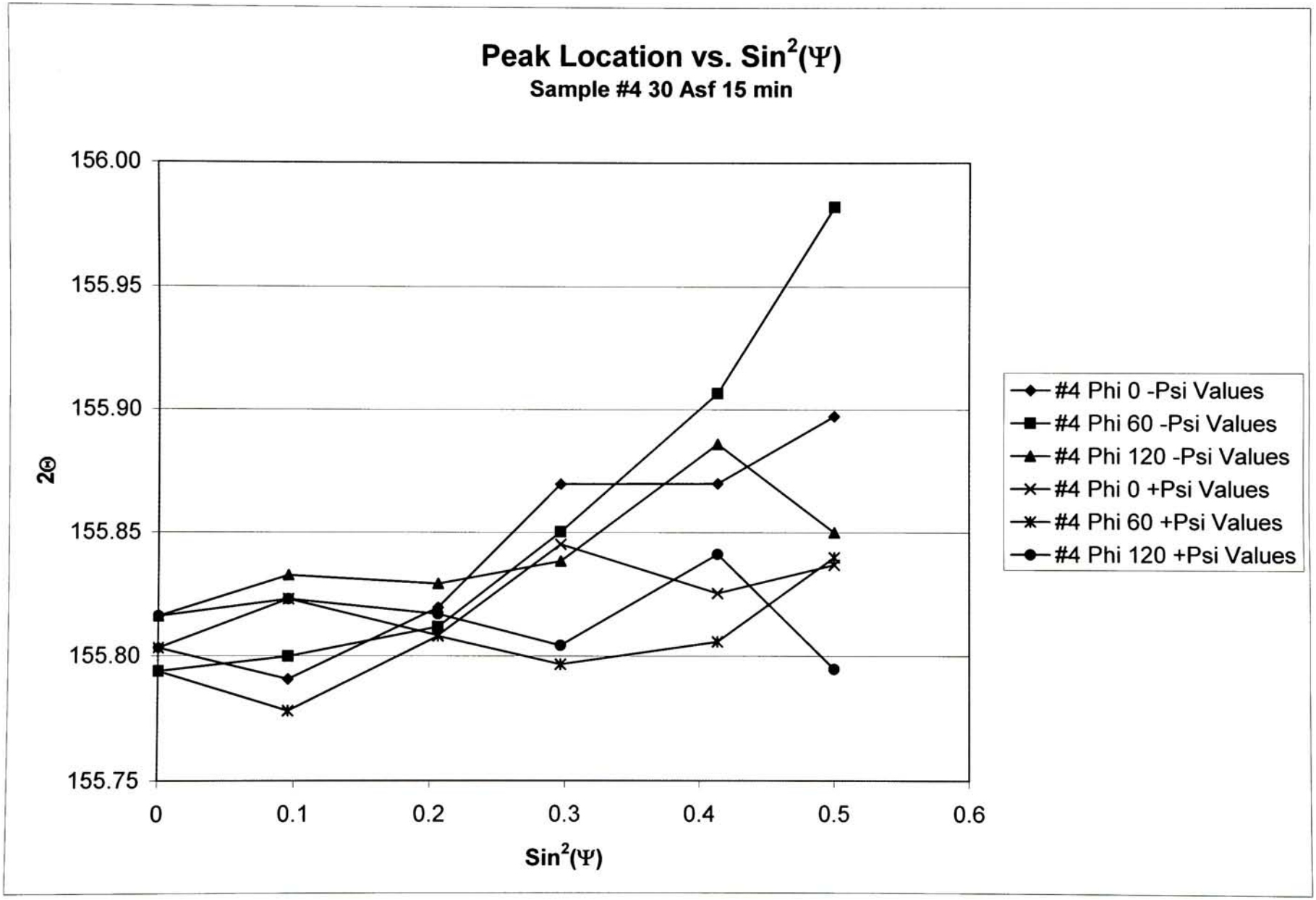

Figure 28: 30 Asf Low Compressive XRD Results (4)

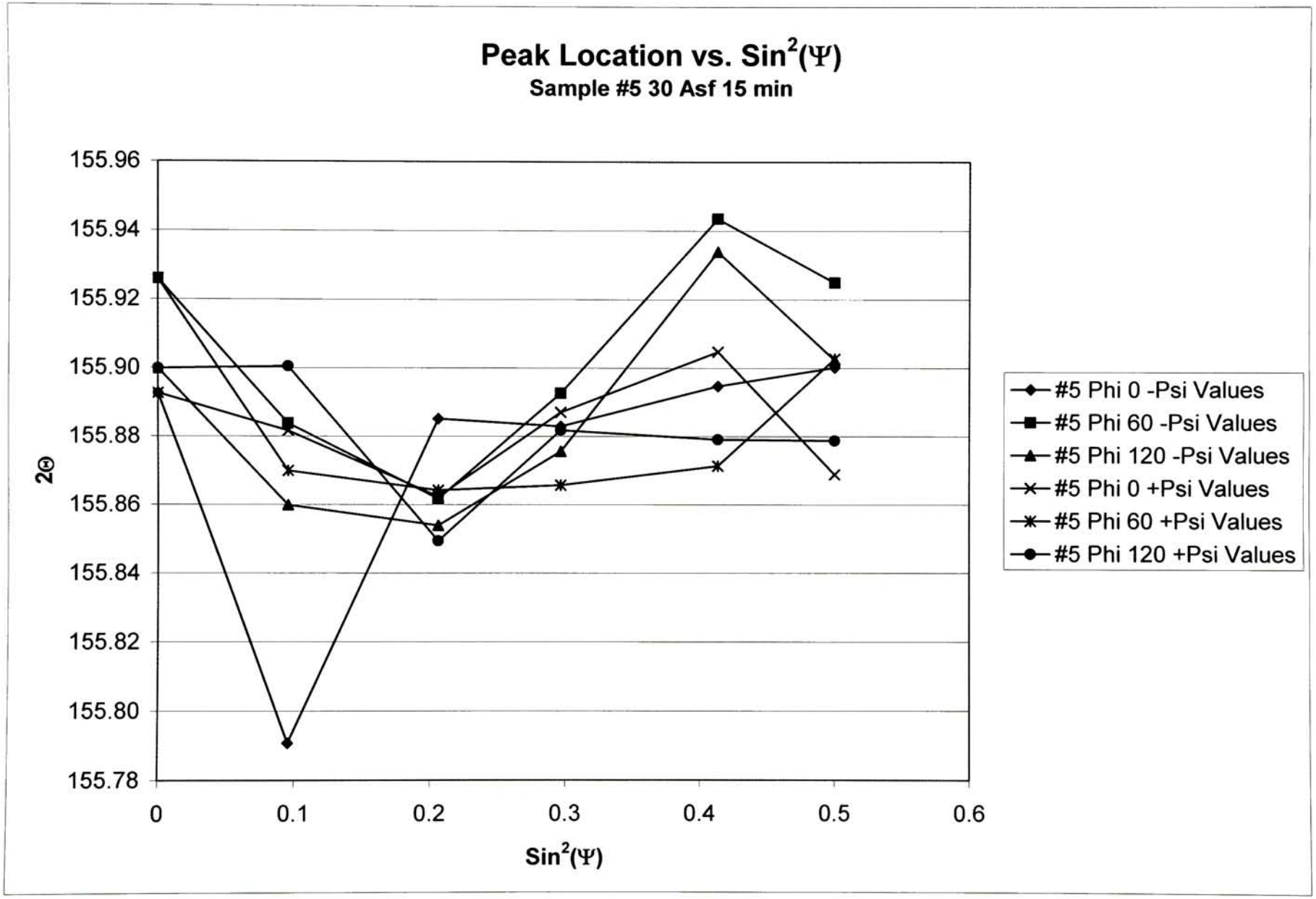

Figure 29: 30 Asf Low Tensile XRD Results (5)

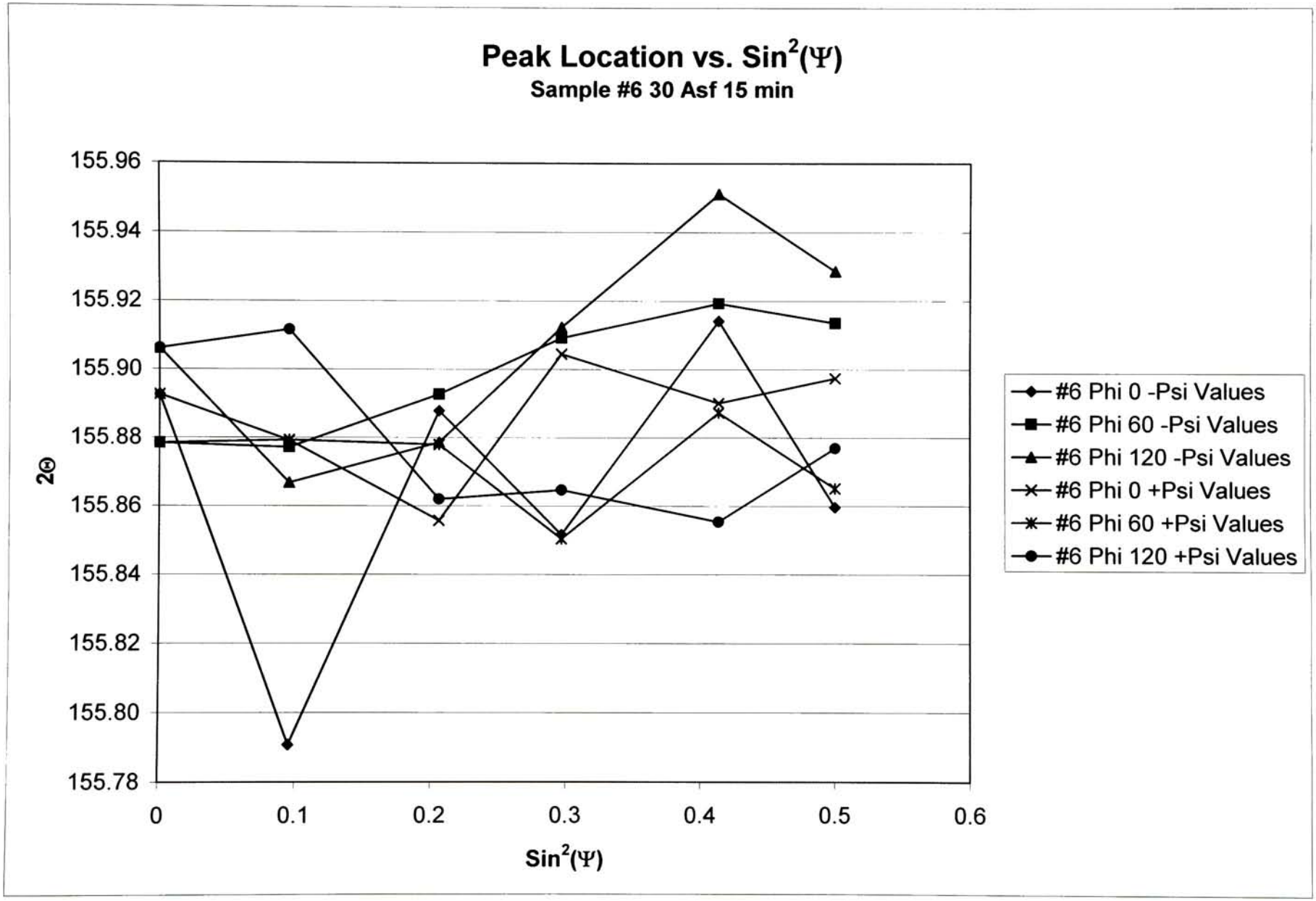

Figure 30: 30 Asf Low Tensile XRD Results (6)

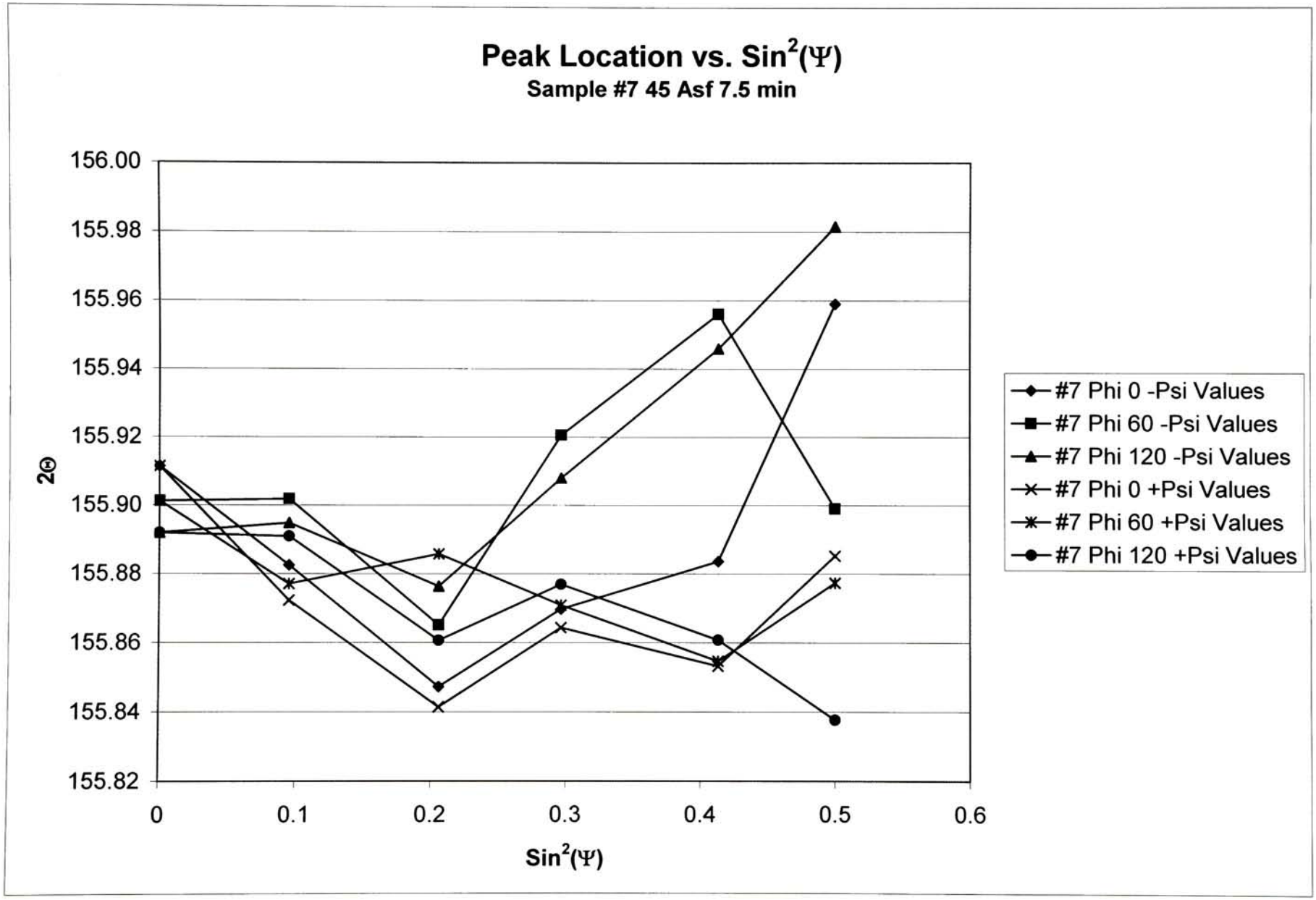

Figure 31: 45 Asf High Tensile XRD Results (7)

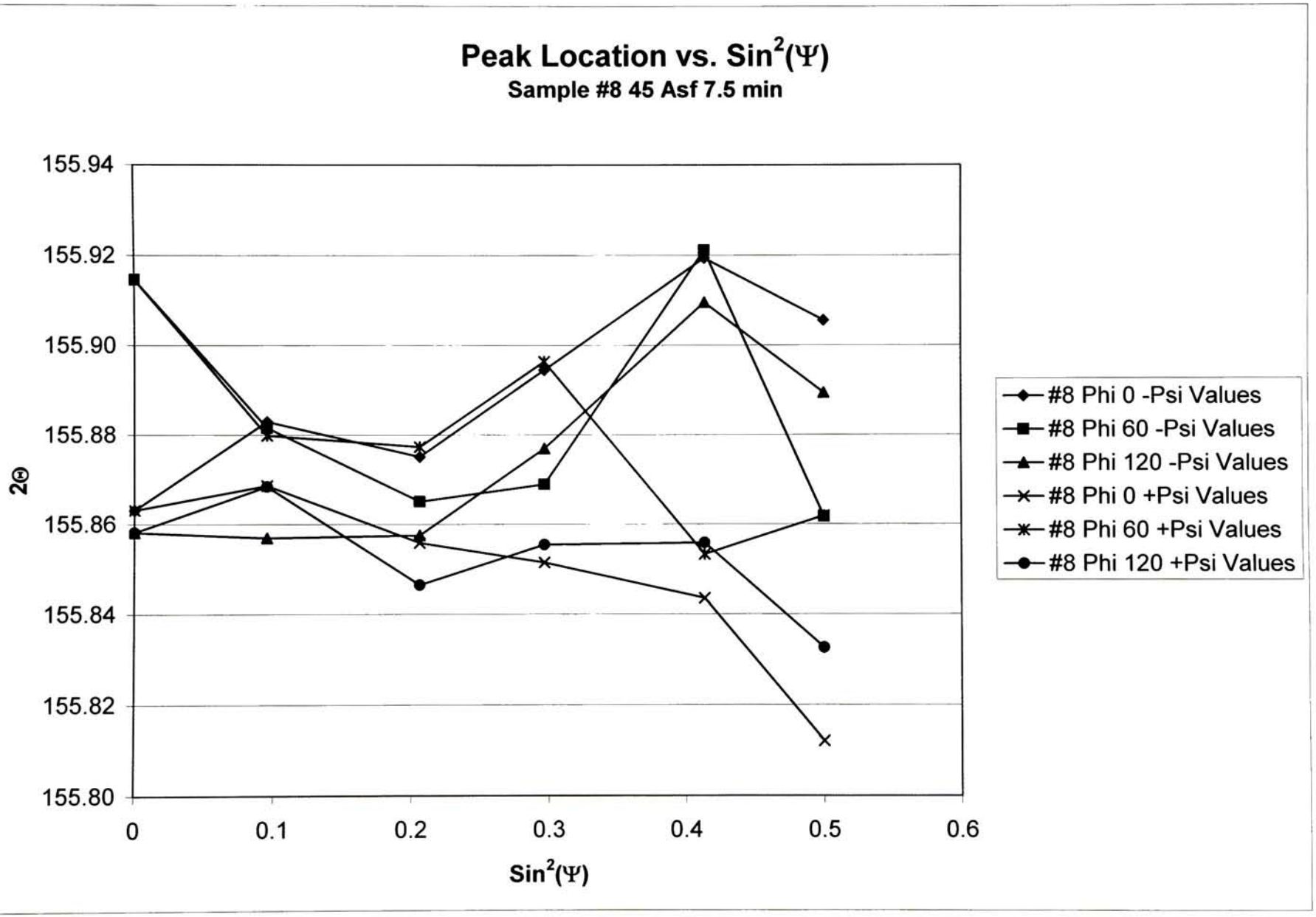

Figure 32: 45 Asf High Tensile XRD Results (8)

Several observations can be made from the Figures 25 through 32. First, the relationship between peak location and $\sin^2(\psi)$ was approximately linear as expected. Figures 25 and 26 display the greatest change in peak location over the range of $\sin^2(\psi)$ measurement locations, indicating that the highest stresses in magnitude occurred in the first experimental condition. The amount of change in peak locations evident in Figures 27 and 28 is slightly less than that of the previous two figures, although a similar linear relationship still exists. This would indicate that a lower residual stress existed in the second experimental condition. Finally, Figures 29, 30,31, and 32 display almost no overall change in peak location over the range of $\sin^2(\psi)$ measurement locations. Therefore the residual stress apparent in the third and fourth experimental conditions was very near zero.

The following table, Figure 33, contains values of residual stress measured in MPa by x-ray diffraction for each of the six samples.

Figure 33: State of Residual Stress as Measured by X-ray Diffraction

Sample Number	σ_1 (MPa)	σ_2 (MPa)	2θ (MPa)	$[\sigma_1 + \sigma_2] / 2$ (deg)
1	-75.92	-101.18	-15.15	-88.54
2	-45.06	-176.48	30.80	-110.77
3	-38.65	-50.90	26.00	-44.78
4	-28.02	-56.70	-30.98	-42.36
5	-2.33	-4.68	8.08	-3.50
6	0.12	-2.89	10.91	-1.39
7	-1.52	-8.83	37.78	-5.17
8	12.30	-4.84	-37.50	3.73

4.4 Comparison of Results

In order to compare measurements made by the two different methods it must be well understood what each method actually measures. In the case of the I.S. Meter, it is obvious from the modeling that the principal stresses acting on the surface of the strip are assumed to be equal. Knowing this, it is apparent that the calculated stress represents the equivalent value of these principal stresses. It is also important to remember that the I.S. Meter with numerical modeling gives the instantaneous stress of each layer, and that although these values have been averaged through part of the deposit thickness there is no compensation made for the fact that the deposit stress is partially relieved as the strip changes length.

The samples measured by x-ray diffraction present altogether different information. Most notably, the x-ray technique allows the measurement of both principal stresses and their orientation while making no assumptions as to the value

of any of these parameters. The x-ray method does not yield values of stress in thin layers as the I.S. Meter does; rather it provides the state of residual stress for the region near the surface of the deposit.

With this information it is possible to reconcile the data obtained from each of these two measurement techniques. First, as the orientation of the first principal stress as determined for each of the eight samples seems to vary almost randomly, it is probably unreasonable to compare either of the two individual principal stresses with any of the stress readings provided by the I.S. Meter. A more sensible approach is to compare these readings to the average of the principal stresses as measured by diffraction and to disregard orientation.

The following table, Figure 34, contains a summary of the data obtained by x-ray diffraction and by the I.S. Meter as analyzed with the numerical model. X-ray diffraction data were obtained by taking the mean of the average of principal stresses for each pair of samples made under each experimental condition.

Figure 34: Summary of Data, Measured Stress in MPa

Assumed State of Stress	Numerical Model Results	X-ray Diffraction Results
Lowest Compressive (15 Asf)	-90.07	-99.66
High Compressive (30 Asf)	-31.46	-43.57
Low Tensile (30 Asf)	21.05	-2.44
High Tensile (45 Asf)	21.95	-0.72

Figure 35: Graph of Summary Data

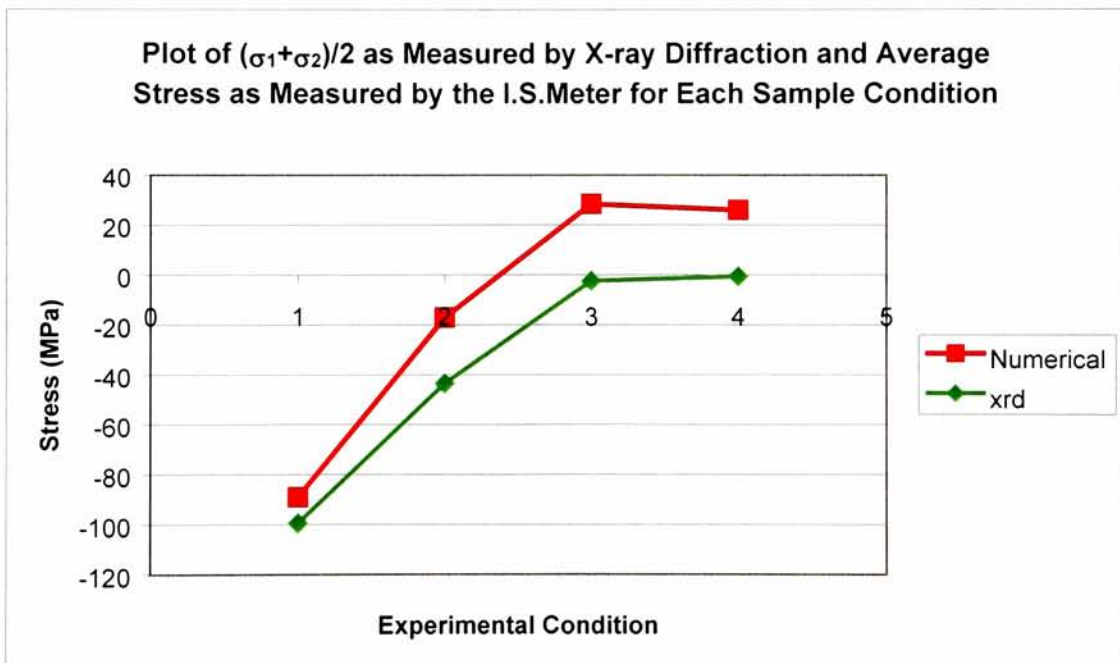

If the assumption is made the copper disks that are plated upon for evaluation of stress by diffraction are rigid with respect to the copper strips that are used in the I.S. Meter, then it follows that the x-ray technique effectively measures the same

instantaneous stresses that the I.S. Meter does. Since the thickness of the disks was approximately 50 times that of the strips (0.10 in. compared to 0.002 in.), it is reasonable to do so. It is therefore feasible to compare the residual stress as measured by x-ray diffraction to the average of the instantaneous stress near the surface as measured by the I.S. Meter with numerical modeling.

Most noticeable when examining the data is the strong agreement between the two methods in the lowest compressive stress ranges. Here, the stress value as measured by the I.S. Meter with numerical modeling is approximately 10% less than the value obtained by x-ray diffraction. As stress increases, the correlation worsens slightly. In the low compressive region the I.S. Meter reads about 25% less than the x-ray results.

The most evident discrepancy between the data obtained from the I.S. Meter and the data obtained by x-ray diffraction occurs in the tensile stress region. Here, there is essentially no stress evidenced by x-ray diffraction while the I.S. Meter records just over 20 MPa. It is encouraging to note the general similarity of results between the 30 and 45 Asf test cases. This demonstrates excellent consistency between the two test methods.

Many factors might contribute to the difference in readings evidenced above. As previously stated, microstresses in the deposit serve to broaden the peaks as determined by x-rays. This leads to a loss in accuracy in determining the location of

each individual peak and therefore an overall loss of accuracy in measuring stress by x-ray diffraction. However, the magnitude of this loss in accuracy is probably not significant enough to cause the significant drop-off apparent in the tensile stress measurements.

Preferred orientation may also play a role in this situation. The assumption that a material is isotropic is based upon the fact that metals are typically composed of many grains having random sizes and orientations. So long as this is the case the true properties of the crystal lattice of the structure, which is anisotropic, are "averaged out" through the volume of the sample and the result is essentially an isotropic solid. Since preferred orientation was evident in the research (relative intensities of certain peaks were diminished greatly at various Ψ angles), it can be assumed that the deposits studied were not truly isotropic.

Another source of error lies in the fact that all material properties used in the calculations (Modulus of Elasticity, Poisson's Ratio) were taken from the Machinery's Handbook with the exception of the modulus of deposited nickel which is known to be softer than that of processed nickel [4]. There was probably a variation between the properties of Copper used in the experiment and the "book values" that they were assumed to be, especially since copper made by two different machining processes was used (rod stock and flat stock). For the purpose of this investigation it was assumed that this approach would be acceptable. The variation between the theoretical material property values and those used is probably rather

small (<10%), and this can be neglected when compared with the rather poor accuracy in measurement achieved by x-ray diffraction.

4.5 Conclusion

The goals of this research have been reasonably satisfied. An improved, numerical model of the deflection phenomenon associated with the change of length method was developed. The results of applying this model to experimental data were compared with that of the traditional models that are commonly used, and there was generally a good correlation between the steady state stress values provided by each method. Additionally, an effort was made to determine the two-dimensional state of stress in deposits by x-ray diffraction and to compare the measured residual stress with the corresponding residual stress as determined by the I.S. Meter with the improved numerical modeling. A fair amount of success was achieved in this endeavor, and although the technique did not provide enough accuracy for the definitive measurement of such low stress levels as this work involved it did demonstrate that the simple I.S. Meter test could effectively measure deposit stress. The I.S. Meter was shown to yield values that are in the same range as those determined by x-ray diffraction and it was shown to yield values that exhibit a strong qualitative correlation to those obtained by x-ray diffraction.

4.6 *Recommendations for Future Research*

This investigation leads to many potential paths of future research. Many other mechanical and material properties of deposits are likely to change with varying internal deposit stress, and studies of these properties might lead to a better means of internal stress analysis. A brief list of these topics might include the magnetic properties of the deposit, the microstructure of the deposit, the microhardness of the deposit, the elastic modulus of the deposit, or possibly the yield strength of the deposit.

Several improvements might be made to the in situ measuring device used for this work, the I.S. Meter. Efforts might be made to reduce the sliding friction of the device, which would reduce the error in the measurements. Similarly, a more accurate instrument could be used to measure deflection through the plating process. Finally, improved x-ray diffraction techniques might add to the accuracy of measurements involved. Exposure time during each scan could be increased, and better means of curve fitting might be used to decrease the error in determining peak locations.

References:

1. R. Weil, The Origins of Stress in Electrodeposits., Plating, December 1970.

2. A. Brenner and S. Senderoff, J. Res. Nat. Bur. Stand., 1949, Vol. 4, No. 2, p. 89.

3. G.G. Stoney, The Tension of Metallic Films Deposited by Electrolosys. Proc. Roy. Soc., (London) A82, 172 (1909).

4. B. Stein, *AESF Electroforming Symposium Proceedings*, Las Vegas, NV, March 27-29, 1996.

5. M. Ya Popereka, Internal Stresses in Electrically Deposited Metals, Indian National Scientific Documentation Centre, New Delhi (1970).

6. S. Dvorak and L. Vrobel, Trans. Inst. Met. Fin. 49 (1971) 153.

7. S. Armyanov and G. Sotirova, Residual Stress Diagrams for Electrodeposition, Metal Coatings Surface Technology, 17 (1982), 321-327.

8. B.D. Cullity, Elements of X-ray Diffraction. 1978, Addison-Wesley, Reading, MA.

9. I. Noyan, Residual Stress Measurement by Diffraction and Interpretation. 1987, Springer-Verlag, New York,NY.

10. J. Dally and W. Riley, Experimental Stress Analysis. McGraw-Hill, Inc., New York, 1991.

Bibliography:

S. Armyanov and G. Sotirova-Chakarova, Internal Stress in Electrodeposited Cobalt, Nickel, and Their Alloys, Part I. Metal Finishing, November 1992 p61-68.B.D.

S. Armyanov and G. Sotirova-Chakarova, Internal Stress in Electrodeposited Cobalt, Nickel, and Their Alloys, Part II. Metal Finishing, March 1993, p42-49.

S. Armyanov and G. Sotirova-Chakarova, Internal Stress in Electrodeposited Cobalt, Nickel, and Their Alloys, Part III. Metal Finishing, April 1993, p59-63.

S. Armyanov and G. Sotirova, Residual Stress Diagrams for Electrodeposition, Metal Coatings Surface Technology, 17 (1982), 321-327.

ASTM B 636-84 Standard Test Method for Measurement of Internal Stress of Plated Metallic Coatings with the Spiral Contractometer.

A. Brenner and S. Senderoff, J. Res. Nat. Bur. Stand., 1949, Vol. 4, No. 2, p. 89.

A. Brenner and S. Senderoff, Proc. Amer. Electroplaters' Soc., 35,53, 1948.

W. H. Cleghorn, K. S. A. Gnanasekaran, and D. J. Hall, Metal Finishing Journal, April 1972.

Cullity, Elements of X-ray Diffraction. 1978, Addison-Wesley, Reading, MA.

J. Dally and W. Riley, Experimental Stress Analysis. McGraw-Hill, Inc., New York, 1991.

H. Dolle, The Influence of Multiaxial Stress States, Stress Gradients, and Elastic Anisotropy on the Evaluation of (Residual) Stress by X-rays. J. Applied Cryst. (1979) 12. 489-501

S. Dvorak and L. Vrobel, Trans. Inst. Met. Fin. 49 (1971) 153.

I. Noyan, Residual Stress Measurement by Diffraction and Interpretation. 1987, Springer-Verlag, New York,NY.

M. Ya Popereka, Zavod. Lab., 27 (1965) 1135.

M. Ya Popereka, Internal Stresses in Electrically Deposited Metals, Indian National Scientific Documentation Centre, New Delhi (1970).

B.Stein, *AESF Electroforming Symposium Proceedings,* Las Vegas, NV, March 27-29, 1996.

G.G. Stoney, The Tension of Metallic Films Deposited by Electrolosys. Proc. Roy. Soc., (London) A82, 172 (1909).

R. Weil, The Origins of Stress in Electrodeposits., Plating, December 1970.

R. Weil, Characterization of Deposits, Coatings, and Electroforms – Internal Stress Part I. Plating and Surface Finishing, September 1997, p56-57.

R. Weil, Characterization of Deposits, Coatings, and Electroforms – Internal Stress Part II. Plating and Surface Finishing, October 1997, p22-23.

R. Weil, Characterization of Deposits, Coatings, and Electroforms – Internal Stress Part III. Plating and Surface Finishing, November 1997, p74-75.

R. Weil, Characterization of Deposits, Coatings, and Electroforms – Internal Stress Part IV. Plating and Surface Finishing, December 1997, p36-38.

R. Weil, Characterization of Deposits, Coatings, and Electroforms – Methods of In-Situ Studies. Plating and Surface Finishing, March 1997, p84-85.